NUMERICAL TRANSIENT THERMAL ANALYSIS OF TIG WELDING ON AISI 304 STAINLESS STEEL

A thesis submitted towards partial fulfillment of the requirements for the degree of

Master of Engineering in Mechanical Engineering

By

AKBAR AZAM

Class Roll No: 002011202018

Registration No: 154317 of 2020-2021

Examination Roll No: M4MEC22018

UNDER THE SUPERVISION OF

SUMAN NIHAR

ASSISTANT PROFESSOR

DEPARTMENT OF MECHANICAL ENGINEERING

JADAVPUR UNIVERSITY

KOLKATA 700032

&

RAKESH BHADRA

ASSISTANT PROFESSOR

DEPARTMENT OF MECHANICAL ENGINEERING

TEZPUR UNIVERSIY, ASSAM- 784028

2022

DEPARTMENT OF MECHANICAL ENGINEERING

FACULTY OF ENGINEERING AND TECHNOLOGY

JADAVPUR UNIVERSITY

KOLKATA – 700032

CERTIFICATE OF RECOMMENDATION

This is to certify that AKBAR AZAM (Class Roll No: 002011202018, Examination Roll No: M4MEC22018, Registration No: 154317 of 2020-2021) has carried out the thesis work titled, **"NUMERICAL TRANSIENT THERMAL ANALYSIS OF TIG WELDING ON AISI 304 STAINLESS STEEL"** under my direct supervision and guidance. I hereby recommend that the thesis be accepted in partial fulfillment of the requirements for awarding the degree of **"MASTER OF ENGINEERING IN MECHANICAL ENGINEERING."**

Countersigned by

……....
Suman Nihar
Assistant Professor
Department of Mechanical Engineering
Jadavpur University
Kolkata-700032

……....
Rakesh Bhadra
Assistant Professor
Department of Mechanical Engineering
Tezpur University
Assam

……..……...…….....
Prof. Amit Karmakar
Head of the Department
Department of Mechanical Engineering
Jadavpur University

..…….…….....
Prof. Chandan Mazumdar
Dean, FET
Jadavpur University
Kolkata-70003

DEPARTMENT OF MECHANICAL ENGINEERING

FACULTY OF ENGINEERING AND TECHNOLOGY

JADAVPUR UNIVERSITY

KOLKATA – 700032

CERTIFICATE OF APPROVAL **

This foregoing thesis is hereby approved as a creditable study of an engineering subject carried out and presented in a manner satisfactory to warrant its acceptance as a prerequisite to the degree for which it has been submitted. It is understood that by this approval the undersigned do not necessarily endorse or approve any statement made, opinion expressed or conclusion drawn therein but approve the thesis only for the purpose for which it has been submitted.

COMMITTEE OF FINAL EXAMINATION ---

FOR EVALUATION OF THESIS

** Only in case the recommendation is concurred

DECLARATION OF ORIGINALITY AND COMPLIANCE OF ACADEMIC ETHICS

The author hereby declares that this thesis contains original research work by the undersigned candidate, as part of his **Master of Engineering in Mechanical Engineering** studies during academic session 2020-2022.

All information in this document has been obtained and presented in accordance with academic rules and ethical conduct.

The author also declares that as required by this rules and conduct, the author has fully cited and referred all material and results that are not original to this work.

NAME: AKBAR AZAM

CLASS ROLL NUMBER: 002011202018

EXAMINATION ROLL NUMBER: M4MEC22018

REGISTRATION NUMBER: 154317 of 2020-2021

THESIS TITLE: "NUMERICAL TRANSIENT THERMAL ANALYSIS OF TIG WELDING ON AISI 304 STAINLESS STEEL".

SIGNATURE: DATE :

ACKNOWLEDGEMENTS

First and foremost, I am deeply grateful to my thesis supervisor Suman Nihar, Mechanical Engineering Department, Jadavpur University & Rakesh Bhadra, Tezpur Universty, Assam for his generous help, valuable suggestion and constant inspiration throughout the period of the thesis work. It will be so good of me to manifest my sincere gratitude to all those who have been by my side during the research period and provide their kind co-operation by guiding me to get this thesis done.

I am grateful to Prof. Head of the Department Jadavpur University for his valuable suggestions during the period of thesis work. I genuinely enjoyed the time spent in Jadavpur University, not only it enriches my knowledge but also the quality time I spent with my friends here.

NAME: AKBAR AZAM

CLASS ROLL NUMBER: 002011202018

EXAMINATION ROLL NUMBER: M4MEC22018

REGISTRATION NUMBER: **154317 of 2020-2021**

2022

ABSTRACT

In the present study, a 3D finite element (FE) model is developed for TIG welding of AISI 304 stainless steel to understand the effect of welding process parameter (welding speed and power) on transient thermal history of the welded samples. The model is developed considering temperature dependent material property and ANSYS platform is used to develop the model. The results from the numerical model indicated that the peak temperature increases with the increase in welding power but peak temperature inversely affected by the welding speed. The peak temperature variation away from the weld line indicated the size of various zones like melt-in zone (MZ), heat affected zone (HAZ) and base metal (BM). The results also indicated that the transient thermal distribution over the welded samples which is the causes of residual stress and deformation. To validate of the model compared with the published experimental results and it is found that its well match with the results from the model.

Keywords: TIG Welding, Numerical Simulation, Heat generation, Transient thermal analysis, AISI 304, Temperature distribution, Peak temperature.

CONTENTS

Chapter 3

Chapter 4

Chapter 5

Chapter 6

LIST OF FIGURES

LIST OF TABLES

Chapter-1

1. INTRODUCTION

Welding is defined as ‘‘a localized coalescence of metals, wherein coalescence is obtained by heating to suitable temperature, with or without the applications of pressure and with or without the use of filler metal’’. The filler metal has a melting point approximately the same as the base metal. The most essential requirement is heat. Pressure may also be employed, but this is not, in many processes essential. In the case of arc welding the work-pieces are melted at the interface and after solidification a permanent weld joint can achieved. Some time a filler material of same or different properties of parent material are used to fill the weld pool. A number of ways and sources are used to perform the welding process like gas flame, laser beam, electric arc, electron beam, ultra sound, friction etc., as per the sources used the welding are given different names like gas welding, electric arc welding, electron beam welding, friction welding ,laser beam welding. It can be done in different environments like under water, open air and also in space. Weld-ability of materials depend upon many different factors like the metallurgical changes of material during welding, changes in hardness of fusion and heat affected zone during rapid solidification, inclusion of flux in case of activated TIG welding process, reaction of material with oxides etc.

1.1 Classification of welding process:

Table1. Different welding process

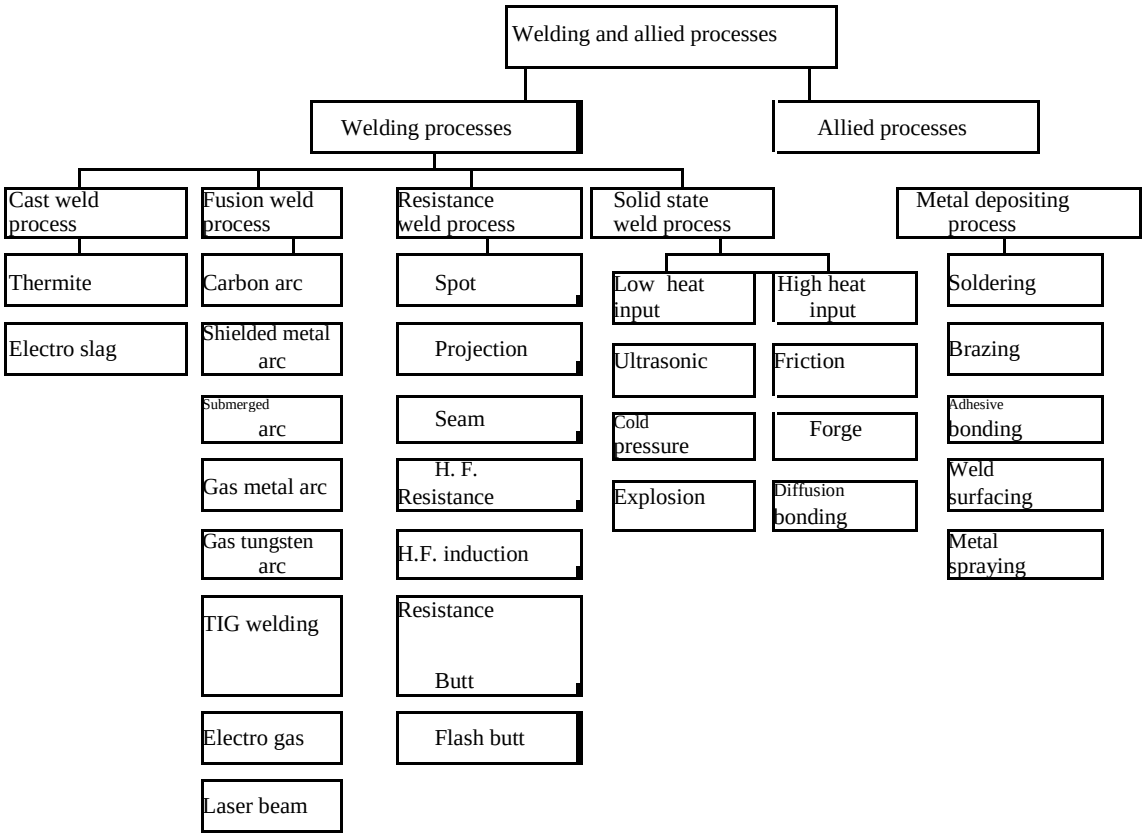

1.1.1 Solid State welding process (Autogenous welding)

In this welding process two work pieces are joined under a pressure and material are heated below the melting point. It is a group of welding process including diffusion welding, explosive welding, ultrasonic welding, cold welding, roll welding etc. The interface atom of the material diffuses to form bond.

a) Ultrasonic welding: The welding uses the ultrasonic energy at high frequency ranges between 20-40 kHz to produce low amplitude mechanical vibration of range 1 - 25 μm. This vibration generate heat at the interface of the specimen which to be welded, that melts the material like thermoplastic and after cooling a permanent weld is achieved.

b) Explosive welding: It is generally used for cladding process of metals and alloys. In this process a detonation of explosive creates a compressive force to join the metal sheets which are overlapped each other. Generally the velocity of detonation and thickness of cladding varies between 1200-7000 m/s and 0.1 - 30 mm respectively.

c) Friction welding: In this welding process heat is generated due to the mechanical friction created by the moving and stationary work piece. A lateral force which is called as "upset" is applied to displace the fused materials.

1.1.2 Resistance welding process

It involves passing an electric current which then changes to heat with high resistance to melt the material to form bond between them. The main advantages of this process is that no filler material is used which make this process coast effective. A clamping force which gives pressure is applied during the heating process which holds the work-pieces in place together until the joint has solidified. There are different forms of resistance welding like projection welding, spot and seam welding, upset welding and flash welding, etc.

a) Spot welding: In this welding process two or more metal sheet are joined by applying pressure and heat obtained from the resistance created between these two contacting metal sheet points from an electric current source.

b) Projection welding: It uses both pressure and electric current to join the metal parts which is designed to meet at one or more specific points with maximum amount of contacts surface. This welding allows more efficient and greater strength welding joins with less energy input.

c) Seam welding: In this welding process two similar or dissimilar materials are joined at the seam which is developed by the electric resistance between two these two materials. The electrode roller is used to give the electric input to the material and also apply pressure to it.

1.1.3 Fusion welding process (Homogeneous welding)

Fusion welding process is also called as liquid state welding process in which the interface of the work pieces are melted with the help of heat to its melting point. In this method of joining the filler material may or may not be used. The filler material may be the same or different from the base material. A heat affected zone is created in the material which to be welded due to the high temperature phase transition.

a) Gas welding: It is a type of liquid state welding process in which gases used as fuel which burn to generate heat. This heat is further used to melt interface surfaces of welding plates or pipes which are held together and after a time it solidifies to form a joint. In this welding process, mostly oxy-acetylene (mixture of oxygen and acetylene) gas is used as fuel gas. It is one of the oldest forms of welding. Because of the gas used this process relatively easy and does not require an expert welder. This process can be done with or without the help of filler material but when the filler material is used it is fed directly into the weld area manually with the help of electrode holder.

b) Energy Beam Welding: In this welding a focused high energy beam either high velocity electron beam or high energy laser beam is used to melt the work pieces. Electron beam welding is performed in vacuum because the atmospheric gases scatter the beam. These types of welding mainly used for precision welding because it does not uses any electrode and welding of advanced material or sometimes welding of dissimilar and hard materials which is very difficult to weld.

c) Arc Welding: In this welding process an electric power supply is used to produce an arc between electrode and the work-piece material which to be join so that the work-piece metals melt at the interface and joint is formed. Power supply for arc welding process can be AC or DC based on the welding process. The electrode used for arc welding could be consumable like in metal inert gas welding or non-consumable as tungsten inert gas welding. For non-consumable electrode an external filler material may be used to fill the weld pool.

i. **Shielded Metal Arc Welding (SMAW)**: This is a type of arc welding process uses metallic flux coated consumable electrode to generate arc between electrode and work pieces. The flux melts together with the electrode and forms a gas and a slag which shield and stabilize the arc and also shield the weld pool from oxidation.
ii. **Gas Metal Arc Welding (GMAW) or Metal Inert Gas Welding (MIG):** In this type of welding process a continuous and consumable metal wire electrode is used to fill the weld pool. A shielding gas generally argon, helium or sometimes mixture of argon and carbon dioxide are used to blow through a welding gun to protect the weld from contamination.
iii. **Gas Tungsten Arc Welding (GTAW) or Tungsten Inert Gas (TIG)**: This is an arc welding process that uses a non consumable tungsten electrode is used to generate arc between electrode and work pieces to melt the interface of the material and after solidification a weld joint is obtained. The weld area is protected from atmosphere to prevent contamination with a shielding gas generally Argon or Helium or sometimes mixture of Argon and Helium and also mixture of argon and carbon dioxide is used. A filler metal may also feed manually or automatically depend upon the thickness of material.

1.2 Mechanism of TIG welding:

In the Tungsten Inert Gas welding, an arc is maintained between a tungsten electrode that is non consumable and the work piece which is to be welded. This arc and the weld pool are protected from atmospheric contamination with a gaseous shield of inert-gas such as argon, helium or argon-helium mixture. The filler metal is optionally used depends upon the thickness of the welding plate. This filler metal can be introduced manually or automatically depends on the process.

The welding power source delivers direct or alternating current depends upon the heat dissipation required for the weld. TIG welding gives better result in welding of difficult to weld materials or hard materials like tungsten and zirconium. TIG welding is used for huge family of materials like aluminum, stainless steel nickel tungsten etc, to achieve high quality welding with the coalescence of heat generated by an electric arc established between a tungsten electrode (non-consumable) and the work piece. Helium and argon gases are the best suited as the shielding gases as they are not chemically reactive. The main aim of shielding gas are to protect the weld pool from surround air to prevent from oxidation and also concentrate and transfers the heat during welding and also helps to start and maintain a stable arc due to low ionization potential.

The electric arc can produce temperatures of up to 20,000 ^{0}C and this heat can be focused to melt and join two similar or different kinds of materials.
Schematic diagram of TIG welding is shown in figure.1.

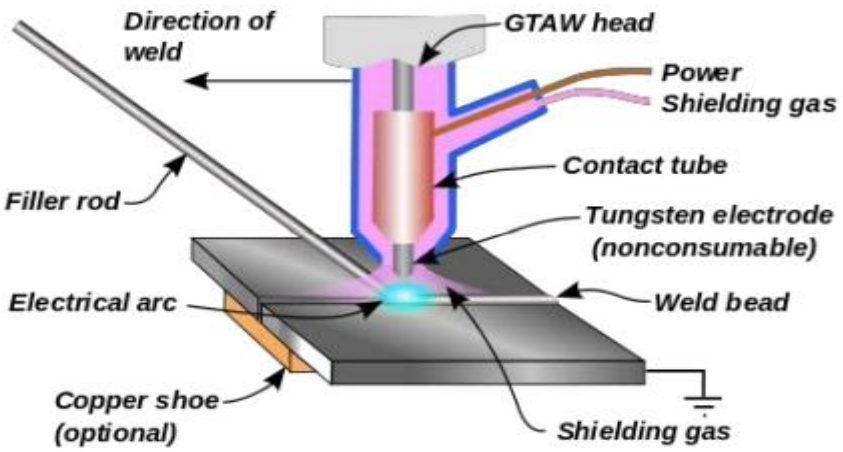

Fig.1 TIG Welding Process [Ansari, Dr.Lokesh [6]]

1.2 TIG Welding Process Parameters:

a) Welding Current: As we know that current is directly proportional to heat this means that as we increase the current then heat input is increased and this heat input applied which affect the weld. Two types current is used i.e. direct and indirect current. Most TIG welding used Direct current on electrode negative means straight polarity. By using this it gives higher penetration and higher welding speed than Direct current electrode positive that means reverse polarity. If electrode is positive then there is more heat generation on electrode and electrode tip degenerates starts.

b) Voltage: Voltage directly proportional to arc length as voltage increases the arc length also increases and if the arc length increases the arc cone gets broader and the penetration decreases. Voltage decreases the arc length gets sorter and the arc cone becomes narrow and the penetration increases. During manual welding it is very difficult to kept the standoff distance constant and if standoff distance vary then the voltage also vary so we have to kept the current constant that's why TIG welding is constant current output method.

c) Welding speed: Keeping current and voltage constant and increasing the Welding speed decrease the heat input and if the Heat input decreases then it decreases the penetration depth and Weld cross section area.

d) Type of Shielding Gas and flow rate: During welding we have to select proper shielding gas and flow rate. The gas used which is not reactive to tungsten electrode and also inert in nature hence Argon, helium and also mixture of Argon-Helium are used. Mainly Argon is used TIG welding process because it is less expansive and gives softer arc. Flow rate are selected according to thickness of material and also types of material.

e) Electrode: As its name implies Tungsten inert gas welding Tungsten electrode is used because of high melting point. TIG Welding is non consumable electrode method means electrode has high melting point enough that non consumed. The electrode size used in TIG welding varies in Length from 75 to 600 mm and varies in diameter from 0.5 to 6.5 mm depends upon Process.

f) Welding torch: In TIG welding the welding torch are developed with cooling system that uses air and water to provide cooling. Water cooling is required in high current welding up to approx 625 A and Air cooling welding torch required in comparatively low current welding approx 225 A. The welding torch has Pipe for Shielding gas flow and in center there is a grip to hold the tungsten electrode.

g) Arc Length: It is also known as Standoff distance i.e. distance from electrode tip and the surface of work piece. Arc length directly affects the voltage if the arc length increases the voltage decreases and depth of penetration decreases vice versa. The Arc length varies from 2 to 5mm according to the Process and types of material and there thickness.

1.4 Advantages of TIG Welding

a) Able to weld ferrous and non-ferrous metals.
b) Makes high quality welds in almost all metals and alloys.
c) Almost none post weld clean up required.
d) The arc and weld pool are clearly visible to the welder.
e) The arc carries no filler, so there is little to none splatter.
f) TIG consumes almost 1/3 of the gas compared to MIG.
g) No slag produced that can be trapped in the weld.
h) Welding can be performed in all positions.
i) No flux is required because inert gas shields molten metal. So no slag and slag inclusion problems.

1.5 Limitations of TIG Welding

a) Very Limited thickness of material can be weld.
b) Tungsten inert gas welding is a time-consuming process - They are slower than any other welding process. Low filler deposition rate.
c) If tungsten transfers to molten weld pool, it can contaminate the same. This inclusion is hard to remove.
d) Safety issue - Welders, are revelation to high intensity of light which can operate eye damage.
e) High initial cost.

1.6 Applications of TIG Welding

TIG welding is used to weld small thickness (3- 6 mm) material. Thicker plates or pipe can also be weld by TIG performing multiple pass but heat input required is more and because of this plate may be distorted and the mechanical properties of base metal also get reduced. It can weld materials like nickel, aluminum, magnesium, copper and their alloys, Stainless Steel like AISI 304, 1020 etc. It can also weld hard materials like titanium, zirconium and their alloys. The TIG Welding process is used in high tech industries like-

- Nuclear industries
- Food processing industries
- Aircraft building
- Automobile industries
- Precision manufacturing industries, etc

Chapter-2

2. LITERATURE REVIEW

TIG welding is one of the newly developed welding processes which have a lot of application in industries. Due to continuously increasing demand of TIG welding in manufacturing industries, needs analysis of the process phenomena. Number of researchers has been doing research on the development of the TIG welding phenomena. Some of the published literature listed below:

Hari Prasadarao Pydi et. al [1] investigated the microstructure, behavior and Al_2O_3 content flux A-TIG weldment of SS-316L steel of cross sections =120 mm x 50 mm x 6 mm; torch angle 10 to 150; Flow velocity argon gas = 3ml/min; five level of current reading are used 100A,80A,60A,50A and 70A; Voltage 250 V. They found that the tensile strength of the base metal (688.842 MPa) is more than the butt welded joint for current 50A (666.858 MPa) welded through filler (316L). Welded joint for the current 80A having low tensile strength(652.82 MPa) as compared to base metal and other butt welded joints. Zala et. al [2] studied the microstructure & mechanical properties of TIG welded aluminized 9Cr-1Mo steel of 55 mm x 10 mm x 5mm. Room temperature taken from 0-25 ^{0}C, efficiency of arc is considered 0.9 and heat input 1.1–1.4 kJ/mm. They found the micro-structural observations that indicated presence of un-dissolved alumina inclusions at the weld fusion line; they observed tensile strength of the weld joint for coated steel is 648 MPa and the weld joint of un-coated steel (667 MPa). Tanmay et. al [3] studied the characterization of Cu–Al alloy lap joint using TIG welding for which Cu and Al are 2 mm thickness, 100 mm and 140 mm length resp.; 4 mm arc length,30^o tip angle, and 5 L/min shielding gas (Argon); welding conducted at different combinations of welding speed (225 mm/min, 250 mm/min, 275 mm/min) and welding current (120 A, 125 A, 130 A, 135 A) they found the good quality weld is at a welding speed of 250 mm/min; average thickness of IMCs formed is 9 mm and 80 mm near Cu and Al plate respectively, Lower current settings (120 A and 125 A) resulted lower tensile strength i.e. for current 120A & speed 250 mm/min and for current 125A & speed 250mm/min due to improper fusion.; the maximum tensile load carrying capacity at 130A & 250 mm/min is 1876 N. Dipali Pandya et. al [4] attempted to explore the effect of hydrogen additions to shielding gas on activated TIG 310 S austenitic stainless steel weld of 6mm thick material Current 182 A Shielding gas flow rate 12 L/min Shielding gas Argon (Ar), Argon + Hydrogen (1% H_2, 2.5%H_2, 4% H_2) Vertex angle of electrode 45 Welding speed 125 mm/min Torch angle 90^o Flux (for A-TIG) SiO_2 Arc length 2 mm. They found the full penetration with 1% volume of hydrogen blend, however, increasing the hydrogen content i.e. 2.5% and 4%H_2 in shielding gas, penetration porosity has been observed. Tensile strength: TIG weld tensile strength 415 MPa; A-TIG weld tensile strength with hydrogen blend 1%, 2.5 % and 4% having tensile strength 482 MPa, 350 MPa and 315 MPa respectively. K.R. Kavitha et. al [5] done experiment to see the mechanical properties of dissimilar materials Titanium grade 5(Ti-6Al-4 V) and low carbon steel (A516) through TIG welding process of thickness of 12 cm; temperature ranges of 600^{0}C -700^{0}C in the interval of 50^{o}C and diffusion timing of 1 hr 5 min under 15KN load in vacuum. They found Tensile strength: obtained for samples S1 (6000 C) is 609.54 MPa, S2 (6500C) is 615.87 MPa and S3 (7000C) is 618.54MPa, Maximum tensile strength achieved at maximum temperature. Hardness: for S1=349.5 HV, S2=339.6 HV and S3=353.1HV. Better hardness was attained at maximum temperature used.

Ansari, Dr.Lokesh [6] studied the process parameter which affects the quality of weld. They used voltage, power, current, welding speed, flow speed of gas as its parameter and draw the relation how these parameters increase or decrease the weld quality. They found that increase in welding current and voltage increase the heat and increase in welding speed decrease the heat generation at the weld surface. Sushant S. Satputaley et. al [7] done experimental to investigation the effect of TIG welding process on chromoly 4130 and aluminum 7075-T6. For tube of Chromoly 4130: OD (outer diameter) 29.21 mm thickness of 1.65 mm and current 66 amps with DCEN filler metal ER70S-2 with OD of 1.6 mm, electrode used was 2% type Ceriated tungsten having an OD of 2.4 mm with a sharp tip. For Al 7075-T6 : OD 25.4 mm and thickness of 3 mm with AC, using filler metal ER5183 with an OD of 2 mm and electrode of Ceriated tungsten having an OD of 2.4 mm with ball pointed tip was used. Amperage setting selected was 1 amp per 0.001 in. of wall thickness. They found that Al 7075-T6 resulted in low weld mechanical properties and does not hold good for welding applications. In General, Al 7075-T6 results in poor weld penetration for high strength. TIG Welding on Chromoly 4130 shows very well weld penetration characteristics without risk of compromising material properties. Aaradhya Bansal et. al [8] attempt to explore the effect of welding parameter on mechanical properties of TIG welded AA6061 of 75 x 55 x 5 mm^3, current 160A, 180A, 190A. Argon gas is used as shielding gas with the flow rate of 10 L/min, maximum load used for test of tensile strength 50 KN. They found, the ultimate tensile strength and yield strength of the un-welded Al6061 are 310 MPa and 270 MPa. The sample welded at 160A has the maximum tensile strength. The hardness is found to be highest for the sample welded at current 190A. The sample welded with the current of 160A had more fine grains and is better suited for the higher tensile properties. The Sample welded with current 190A showed good bending strength. Peter Omoniyi et. al [9] performed TIG welding of Ti6Al4V alloy: Microstructure, fractography, tensile and micro hardness are calculated for 2-3 mm thick material of Ti6Al4V alloy. Argon gas used for (3mm thick): E31 Current(A) = 100 and Gas flow rate(L/min) = 9 ; E32 = 120 and 9; E33 =120 and 12 ; E34 = 100 and 12; For(2 mm thick): E21= 60 and 9; E22 = 50 and 9 ; E23 = 50 and 7 ; E24= 60 and 7 resp. They found that for (3mm thick material): maximum elongation at maximum gas flow rate and minimum current used. At weld zone, maximum micro-hardness at maximum current and minimum gas flow rate used for 3 mm thick material. For (2 mm thick material): elongation is maximum at E24 and decreases more rapidly in decreasing with the current and also decreasing with increasing of gas flow rate. At weld zone, maximum micro-hardness at minimum current and maximum gas flow rate used for 2mm thick material. Ramakrishnan A. et. al[10] performed experimental investigation on mechanical properties of TIG welded dissimilar AISI 304 and AISI 316 stainless steel using 308 filler rod with plates of 3 mm thickness with Butt joint; They used filler material AISI 308L of 2.5 mm diameter Current are 30 A, 45 A, 60 A for AISI 304 and Voltage 40 V, 60 V and 80 V are used for AISI 316 material. Inert gas used is Argon. They found the maximum ultimate tensile strength for the specimen that is welded with maximum current. The hardness value at the weld zone in the specimen 2 i.e. AISI 316 with 45 A is the highest for the set of readings used for the experiment. The overall hardness of the heat affected zone (HAZ) was higher than that of the hardness of the base metal. The specimen 3 for TIG welded with 60A current shows the highest Ultimate tensile strength of 528.36 MPa. The microstructure of the weld zone in the specimen 2 with 45A current is well distributed and also finer microstructure is observed. Bo QIN et. al [11] studied the Microstructure and mechanical properties of TIG/A-TIG welded AZ61/ZK60 magnesium alloy joints of size 80 mm × 40 mm × 3 mm; 99.99% argon with gas flow rate is 7.5 L/min, Speed is 180mm/min, Stand-off

distance is 2mm, Welding current is 60, 70, 80, 90, 100 A; For A-TIG welding TiO_2 particles used as a flux. They found that HAZ (heat affected zone) exhibited larger grains and the FZ (Fusion Zone) presented more refined grains. The refined grain size in the FZ of the TIG welded AZ61/ZK60 magnesium alloy joints was calculated to be about 19μm. Maximum tensile strength is 207 MPa at current of 80A. The TiO_2 coated sample shows a maximum tensile strength of 156 MPa, which was 24.5% lower than uncoated specimen. Anand Baghel et. al [12] done experiment to study the effect of oxide and chloride fluxes on microstructure and mechanical properties of joints in activated flux TIG welding of dissimilar SS202 and SS30 alloys of size 90 mm x 50 mm x 3 mm. Fe_2O_3 oxide flux and $CaCl_2$ chloride flux are used. Current (A) is 80, Feed Rate (mm/Sec) is 3.5, Speed (mm/sec) is 10, Shielding gas flow rate (L/mm) is 5. They found that aspect ratio (D/W) is more in Fe_2O_3 oxide flux; Complete penetration only achieved in Fe_2O_3 oxide flux; DOP maximum in Fe_2O_3; Maximum hardness in fusion zone on material SS304 and minimum in TIG welding(without use of flux); They also found that the fine grained heat affected zone(FGHAZ) hardness was higher than coarse grain for all welding conditions. Anup Kulkarni et. al [13] studied the microstructure and mechanical properties of A-TIG welded AISI 316L SS-Alloy 800 dissimilar metal joint for Current 230 A, Arc voltage is 15-16 V, Arc length (3 mm) Travel speed 80 mm/min, Heat input (η =70%) is 1.87 kJ/mm, Shielding gas (Flow rate) for Pure argon (99.99%) is 10 lit/min Electrode diameter is 2.9 mm, Electrode included angle 60 deg. They found the aspect ratio (0.68). A-TIG welded AISI 316L SS-Alloy 800 joint exhibits full thickness penetration in 8 mm thick plates without any solidification cracks or defects. Highest hardness is found at unmixed zone. A-TIG weldment exhibits the ultimate tensile strength of 514 MPa with a joint efficiency of 91% (with respect to Alloy 800 base metal). Qingdong Qin et. al [14] done experiment for microstructures and mechanical properties of TIG welded Al-Mg_2Si alloy joints of size 80 mm × 80mm × 2 mm; In this experiment AC Arc welding with 2 mm diameter tungsten electrode is used; Argon gas as an inert gas, current is 125A, 135A and speed is 10mm/s. They observed that the low-angle grain boundaries (LABs) in the base material (BM) transformed into high-angle grain boundaries (HABs) in the fusion zone (FZ). The joints welded at 125 A and 135 A exhibited similar hardness characteristics, and the hardness in the FZ was 45% higher than that in the BM (Base metal). The UTS of the joints welded with 135 A was approx same to that of the BM and higher than that of the joints welded with 125 A current. Kamlesh Kumar et. al [15] studied the effect of Activated Flux on TIG Welding of 304 Austenitic Stainless Steel of 3 mm thick; TiO_2, Al_2O_3 and CaF_2 were used as flux; 2.4 mm diameter tungsten electrode were used and stand-off distance is 3 mm; pure Argon gas was used; current is 120A; Speed is 3.5mm/s and Gas flow rate is 18 L /mm. They found that weld penetration depth enhanced approximately 75% for using TiO_2 as a flux and 10 % for Al_2O_3 flux as compared to C-TIG (conventional TIG) welding. Whereas, for using CaF_2 as a flux the weld penetration depth reduced, Aspect ratio improved significantly for using the flux TiO_2. The micro-hardness value of the welded using A-TIG was also more than the sample produced in C-TIG. High hardness achieved for using TiO_2 and CaF_2 flux, using Al_2O_3 flux has same hardness as C-TIG. Habibur Rahaman Hazari et. al [16] performed a experimental investigation of TIG welding on AA 6082 and AA 8011 of 1.5 mm thick material. ER 4043 was used as a filler rod with varying diameters of 1.6 mm, 2 mm & 2.5 mm along with argon with a variable flow rate of 6, 7 & 8 L/min as a shielding Gas and welding currents of 80, 100, & 120 Amps. They found that Maximum ultimate tensile stress (170.25Mpa) and minimum hardness (37.26HRB) with Filler rod with diameter 2.5mm, current 120A and Gas flow rate 8 L/min; Lowest Ultimate tensile stress (98.25Mpa) and high hardness (68HRB) with filler rod of diameter 1.6mm,

current 80A, Gas flow rate 6L/min. The ultimate tensile stress (UTS) is increases with increase in current and gas flow rate. Maximum hardness are achieved for 80 A of current with a gas flow rate of 6 L/min. Jipeng Shi et. al [17] studied the effect of active gas on weld appearance and performance in laser-TIG hybrid welded of titanium alloy. The parameters taken as Laser pulse energy (Q) is 13 J; Wire feed rate(s) is 1700 m/min Laser pulse frequency (f) is 30Hz,TIG current (I) is 170 A Gas flow speed (q) is 15 L/min ; Welding speed (v) is 525 mm/min, Electrode height (H) is 2mm, CO_2 content(vol. %) is 0,1, 2, 3. They found that H/W increases first and then decreases with CO_2 content increases from 0% to 3%. Thickness of oxide layer increase from 23 mm to 50 mm with the increase of CO_2 content from 0% to 2% after that remain constant for 3% of CO_2; Maximum Tensile strength found at 2% is 1057 MPa. M. Junaida et. al [18] performed a comparative study of pulsed laser and pulsed TIG welding of Ti-5Al-2.5Sn titanium alloy sheet. The parameters set for P-LBW: Current is 260A, Pulse duration is 8 ms Pulse frequency is 8 Hz, Speed is 160 mm/min and Stand of distance is 4 mm; For P-TIG: Current that is Primary (32A) and background (16A), Pulse width for High (8 ms) and Low (4 ms), voltage is taken as 10V Speed is 32.5 mm/min and Arc length is taken as 4 mm. They found that the width of weldment for P-TIG is more than P-LBW because of the higher heat input used in P-TIG welding. For P-TIG weldments, the equiaxed grains of PM (parent metal) became larger in size in the HAZ and FZ. In P-LBW at FZ, hardness is approx 26 HV which is more than that of FZ at P-TIG weldment. UTS in P-LBW are found to be 15 MPa more than that of P-TIG and it is 95.5% of base metal. Muhammad Samiuddin et. al [19] investigated the process parameters of TIG-welded aluminum alloy through mechanical and micro-structural characterization on plates having dimension of 15 x 300 x 180 mm^3. The parameters are taken as: filler diameter is 2.4 mm, tungsten diameter is 3.2mm and Shielding gas flow rate is 8-10 L/min, Filler rod angle in X-axis 20-30 deg. Torch angle in X-axis 70-90 deg and in Y-axis is 90 deg. Current is taken as 175, 220, 270, 320, 360, 385A, Voltage is 24, 24, 22, 20, 18, 18V, Heat Input(KJ/mm): High= 3 to 5, Medium=1 to 2, Low= <1, Torch speed (mm/sec) is less than 1, 2-4, 5-6 resp. They found that the optimum heat input value to weld a thick plate of Al-5083 alloy was found to be 1-2 kJ/mm with 270-320 A welding current and 2-4 mm/s torch traveling speed. Using MHI (medium heat input) only 18.26% of strength was lost. PMZ (partially melted zone) found to be widened with the increase of heat input. The grain size of PMZ was found to be coarser than that of the respective grain size in the fusion zone. R. S. Vidyarthya et. al [20] evaluate the weld ability of 409 FSS with A-TIG Welding Process for thickness of 8 mm welding currents are 100 A, 130 A, and 160 A flux coating density 0 to 7.13 mg/cm^2 Speed is 120 mm/min and flux used are SiO_2 and Cr_2O_3. They found the maximum DOP with SiO_2 and Cr_2O_3 were 4.9 mm and 4 mm, resp. Maximum D/W ratio of 0.71 was found at 160 A with SiO_2 as flux. They also found the increase in the depth of penetration from 2.23 mm to 4.7 mm with increase of the flux coating density from 0 mg/cm^2 to 2.5 mg/cm^2. Further increase from 2.5 mg/cm^2 up to 7.13 mg/cm^2 does not increase the DOP. Maximum depth of penetration was achieved by using 2.5 mg/cm^2 as flux coating density. Minimum width is found at 6.23 mg/cm^2, maximum D/W are found at 4.27mg/cm^2. The depth of penetration and depth to width ratio increases with increase in the welding current. SiO_2 flux was found more effective to increase the depth of penetration and depth to width ratio. Optimum range of flux coating density was found to be 2mg/cm^2 to 4.5 mg/cm^2.

Chao Chen et. al [21] investigated the formation microstructure of Ti-6Al-4V weld bead during pulse ultrasound assisted TIG welding with the thickness of 3 mm. The parameters are taken as Welding current, Welding speed, Welding voltage, Shield gas flow (Ar), Tungsten diameter are 90A, 5 mm/s, 12V, 15 L/min, 3.2mm resp. Ultrasonic frequency is 20 kHz, Ultrasonic radiator height (URH) is 12 mm. For pulsed frequency greater than 10Hz: they found the weld penetration and weld width of PU-TIG were increased by around 46% and 27%, resp. The minimum grain diameter of 148μm was obtained in the PU-TIG for the pulsed frequency of 10 Hz. In the PU-TIG, the maximum average hardness was found to be 376 Hv at 10 Hz pulse frequency. Jun Shen et. al [22] done experiment to study the effects of welding current on properties of A-TIG welded AZ31 magnesium alloy joints with TiO_2 coating. The dimensions used are 100 mm×50 mm×6 mm. The welding current used for different specimens are 110 A, 120 A, 130 A (without TiO_2 coating), and 130 A, 140A, 150A (with TiO_2 coating) respectively. Welding voltage is (15±0.3) V, welding speed of 300 mm/min and shielding gas argon are used of flow rate 15 L/min. They found that the TIG welded joint with TiO_2 coating shows a deeper weld penetration and larger grain size with respect to the welded joint without TiO_2 coating by using 130A current. They also found that increasing the welding current leads to increase the D/W ratio. S.P. Lu et. al [23] attempted to explore the efficient TIG welding of $Cr_{13}Ni_5Mo$ martensitic stainless steel. The double-shielded TIG welding process was adopted in the experiment to weld 9 mm thick plates in a single pass. He (Helium) is used as inner shielding layer gas and mixture of He and Co_2 is used for outer shielding layer gas. Parameters used as the welding speed which is in the range of 1.5–5 mm/s, the welding current is in the range of 120–240 A, and the electrode gap is in the range of 1–7 mm. They found that the double-shielded TIG welding process shows an efficiency of 2–4 times greater than that of Conventional TIG welding. This process not only allows for higher weld efficiency as compared with the Conventional TIG welding but also produces better weld impact properties than that of Metal active gas welding.

J.L. Song et. al [24] done experiment to study the effects of Si additions on inter metallic compound layer of aluminum–steel TIG welding-brazing joint of thickness 3 mm. The welding parameters are welding current 135A, arc length 3.0–4.0 mm, welding speed 120 mm/min, argon gas flow rate 8–10 L/min. They found that addition of Si minimize the IMC layer thickness and addition of 5% by wt. of Si, the IMC layer achieved the optimum mechanical properties and the tensile strength of joint becomes 125.2 MPa. Sudhanshu Ranjan Singh et. al [25] studied A-TIG (activated flux tungsten inert gas) welding: – A review of Titanium Plate of 6 mm thick. Speed used is 100 mm/min, current is 105 Amp and Shielding gas used is Helium. They found that greater roughness in the case of A-TIG welding because the oxide particles entrapped in weld zone of the specimen. Gap of 200MPa is present in-between C-TIG and A TIG samples during evaluation of tensile strength. A-TIG has higher hardness value which might be the results of higher peak temperature and rapid cooling rate. Flux usage in the case of A-TIG welding has no effect on the ductility of the welded part of the specimen. Hemant Kumar, N K Singh [26] attempted to explore the performance of activated TIG welding in 304 austenitic stainless steel welds of size 150 mm x 50 mm x 8 mm. The welding parameters used in this experiment are current 80-160 A, arc length is 1.5 mm, gas flow rate is 10 l/min and the welding speed used is 100 mm/min. The Six different types of oxides were used i.e. Cr_2O_3, FeO, Fe_2O_3, MoO_3, SiO_2, and Al_2O_3 to see the effect of oxide flux on different mechanical properties also on the weld morphology and microstructure of the weld joint. They found that all the oxide powders increases the depth of penetration except Al_2O_3. Maximum penetration is by using

SiO_2. Microstructures are different in C-TIG and A-TIG welding because of difference in the cooling rate. There is not any significant change in the hardness of A-TIG while comparing with the C-TIG. Pratishtha Sharma et. al [27] successfully performed A-TIG welding of dissimilar P92 steel and 304H austenitic stainless steel of 8 mm thickness to study Mechanisms, microstructure and mechanical properties. Electrode type is tungsten with 2% ThO_2. Parameters taken are Electrode diameter is 2.9 mm, Electrode vertex angle is 60°, Power supply type DCEN with welding current of 220 A, Welding speed is 80 mm/min, Arc length is 3 mm and shielding gas and flow rate- 99.99% Pure Ar and 10 L min^{-1}resp. The four different oxide fluxes are used which are Cr_2O_3, MoO_3, SiO_2 and TiO_2. They found that the use of TiO_2 oxide flux resulted in highest depth of penetration of 9.39 mm and D/W ratio of 0.93. They observed wider HAZ of width 5 ± 2 mm at P92 steel side whereas only 150 ± 50 μm was found in 304H ASS side. In this experiment the highest hardness of 396 ± 11 HV is observed at the P92 CGHAZ (Course grain heat affected zone). Rakesh Bhadra et. al [28] investigated the thermo mechanical analysis of CO_2 Laser Butt Welding on AISI 304 Steel Thin Plates using ANSYS-14.5. The dimensions of plate are taken as 100 mm × 100 mm × 1 mm. The welding parameters used are laser scanning speed (300, 400 and 500 mm/min) and laser power (1300, 1500 and 1700 W). They found after performing both numerical and experimental analysis that maximum variation of 3.74% in the peak temperature. They also found that peak temperature, fusion zone (FZ) and heat affected zone (HAZ) is directly proportional to laser power and inversely proportional to welding speed means these all three increase with increasing of laser power and also increases with decreasing of laser welding speed. Pramod Kumar et. al [29] successfully performed the numerical modeling of TIG welding of austenitic stainless steel (304L) .The FEM model used in the current numerical simulation is designed for 320 mm x 100 mm x 1.4-mm-size of 304L steel sheet. The parameters set as Welding current are 25A, 75A, 115A, 145A.Welding Voltage is 15V. Welding speed is 7 mm/sec. They found the maximum peak temperature at welding of 145A current is 2248 K and lowest peak temperature obtained at 30 A current is 756 K at X = 2 mm away from the weld line. At each welding current used the peak temperature decreases away from the weld line. They also found that the peak temperature increases with increase in welding current at a fixed welding speed and voltage. Ravisankar et. al [30] performed numerical Simulation with experimental validation in TIG welding with varying welding speed and power to study the temperature distribution and residual stress. They found the optimum heat input of 300 J/mm. The best combination of welding speed(1 mm/sec) and Power of 300 W they got which gave good penetration with controlled fusion and heat affected zone at maximum temperature of 1960^oC. For the case of 3 mm location away from the Welding Center, tensile stress increases and was found to be 150 MPa on the inner surface, and the compressive stress also increases and found to be 100 MPa on the outer surface. Zhi Zeng et. al [31] studied the Numerical and experiment analysis of residual stress on magnesium alloy and steel butt joint by hybrid laser-TIG welding. The thickness of magnesium alloy sheet (2.2 mm) which is more than that of steel sheet (2 mm). The TIG welding parameters set as Welding speed (mm/min) is 600 TIG current (A) is 120 and Arc length (mm) is 2.5 and the Hybrid welding parameters taken as Welding speed is 1500mm/min TIG current 80A Laser power is 400W Defocus distance 1mm Angle between tungsten electrode and work piece 50^0 Laser frequency (Hz) 20 Hz Flow rate of shielding gas 15 L/min. They observed that the temperature distribution at the hybrid weld region is exposed to faster rate of heating and cooling in hybrid welding than Conventional TIG welding. The residual stress is 20% less in hybrid welding as compared to TIG welding.

Farid et. al [32] analyzed the numerical simulation of the T-Shaped fillet welds of AISI 304 and AISI 1020 steel plate of 5mm,6mm,8mm thickness plate. The parameters used are current(A) is 90 ± 3% Voltage (V) is 28 ± 4% and Welding speed(mm/sec) is 2.34 for each plate of AISI 304 material and for AISI 1020 these parameters are 103 ± 5%, 24 ± 5% ,1.75 resp. The length of leg in each case is 5mm. They found that the lowest error of 10.4% for the plate of 5mm thickness of AISI 304 is achieved and errors of 0.36% for the plate of 5mm thickness of AISI 1020 are found when comparing with numerical simulation.

2.1 Gaps from the literature

There are vast numbers of literatures available on TIG welding techniques to be used while welding of austenitic steel AISI 304.

Few numbers of literature available on the transient thermal analysis on TIG welding of AISI 304 stainless steel.

No literature is available on the numerical model considering volumetric heat source as heat generation on the steel.

2.2 Objectives

The main objectives of the present work is

1) To develop a numerical FEM thermo-mechanical model with the help of ANSYS software package considering the temperature-dependent material property of AISI 304 stainless steel.

2) To determine the effect of different welding process parameters (welding power and welding speed) on the welding quality.

3) To validate the FEM model

Chapter-3

3. MATERIAL PROPERTIES

The material used in the experiment and numerical simulation is AISI 304. The chemical compositions of the AISI 304 are shown in Table 2.

Table 2 Chemical compositions of AISI 304 Steel. [Rakesh Bhadra et. al [28]**]**

Elements	Ni	Cr	Fe	C	Mn	Si	S	P	Mo	Cu
%by weight	8.9	18.4	71.2	0.06	1.06	0.34	0.011	0.03	0.05	0.05

The thermal properties that is Specific heat (J/g °C), Conductivity (W/mm °C) and Density (g/mm^3) and mechanical properties that is Yield stress (MPa), Young modulus (GPa) and Poisson's ratio area listed in the Table 3 and 4 respectively.

3.1 Thermal Properties

Table 3 Thermal Properties of AISI 304 Steel. [Farid et. al [32]]

Temperature (^{0}C)	Specific heat (J/g °C)	Conductivity (W/mm °C)	Density (g/mm^3)
0	0.462	0.0146	0.790
100	0.496	0.0151	0.788
200	0.512	0.0161	0.783
400	0.525	0.0179	0.779
600	0.540	0.0180	0.775
800	0.577	0.0208	0.766
1000	0.604	0.0239	0.756
1200	0.676	0.0322	0.737
1400	0.692	0.0337	0.732
1500	0.700	0.1200	0.732

We can see the trend from above thermal properties table and found that specific heat is lowest at 0^{o}C and increasing with increase in temperature. The conductivity of AISI 304 is increasing with increase in temperature and the density of AISI 304 is decreasing as we increase the temperature.

3.2 Mechanical Properties

Table 4 Mechanical properties of AISI 304 Steel

Temperature (^{0}C)	Yield stress (M Pa)	Young modulus (G Pa)	Poisson's ratio
0	265	198.5	0.294
100	218	193.0	0.295
200	186	185.0	0.301
400	170	176.0	0.310
600	155	167.0	0.318
800	149	159.0	0.326
1000	91	151.0	0.333
1200	25	60.0	0.339
1400	21	20.0	0.342
1500	10	10.0	0.388

Chapter-4

4. MODEL METHODOLOGY

A 3-D numerical simulation of TIG welding process is done with the help of ANSYS APDL Software of AISI 304. In this numerical simulation the effect of welding speed and heat power are studied and with the help of this temperature distribution are noted down and the temperature curve are plotted with respect to time and distance away from weld line.

4.1 Thermal Analysis

The heat energy governing differential equation with heat generation for homogenous, isotropic solid (Pramod Kumar et. al [29]) in rectangular coordinate are given as

$$\frac{\partial}{\partial x}\left(K\frac{\partial T}{\partial x}\right) + \frac{\partial}{\partial y}\left(K\frac{\partial T}{\partial y}\right) + \frac{\partial}{\partial z}\left(K\frac{\partial T}{\partial z}\right) + Q(x,y,z) = v\rho c\frac{\partial T}{\partial y} + \rho c\frac{\partial T}{\partial t} \quad (1)$$

Where, K= thermal conductivity of the material (W/ mm ^{0}k), Q = Heat source that is heat generation in unit volume (J/mm^3), c = specific heat of the material (J/kg k), v = welding speed (mm/ min), T= Temperature in ^{0}k, ρ = density of the material (kg/mm), t = time in minute.

The governing differential equation without heat generation for homogenous, isotropic solid is taken from Rakesh Bhadra et. al [28] are expressed as

$$\frac{\partial}{\partial x}\left(K\frac{\partial T}{\partial x}\right) + \frac{\partial}{\partial y}\left(K\frac{\partial T}{\partial y}\right) + \frac{\partial}{\partial z}\left(K\frac{\partial T}{\partial z}\right) = \rho c\frac{\partial T}{\partial t} \quad (2)$$

Where, ρ = Density of the material, c = Specific heat, T= Temperature, K = Thermal conductivity of the material and t = Time

To solve the above governing differential equation we need the boundary condition. Following are the boundary condition:

a) The first condition is the Initial condition

We all know that when we start the welding the Temperature of the plate is equal to the ambient temperature. We can write this expression as:

$T = T_\infty$ at $t = 0$ (3)

Where, T_∞ = Ambient Temperature and t = time

b) From energy balance

We know from energy conservation energy neither be created and nor be destroyed it means that the energy in is equal to energy out. Here heat is in the form of energy we write the equation from this energy conservation.

Heat supplied = Heat loss

Let the surface area of the plate is S and q_n is heat flow vector per unit area in normal direction and q_{sup} is heat supplied per unit area then we write the equation as:

$$q_n = q_{sup} \quad (4)$$

Where q_n , q_{sup} are heat in normal direction and heat supplied per unit area (W/ mm^2). Further q_n can be written in the form of unit normal vector

$$q_n = \{q\}^T \{n\} \quad (5)$$

Where {n} = unit normal vector pointing outward

c) From Newton's law of cooling:

Newton states that heat loss due to convection is directly proportional to the difference in the temperature. From Newton's law of cooling, $Q \propto \Delta T$

$$Q = h\,(T - T_\infty) \quad (6)$$

Where, T = Temperature of the plate, T_∞ = Ambient Temperature, h = Convective heat transfer coefficient in W/ m^2K

4.2 FE Modeling Details

In this modeling SOLID70 thermal element are used because of good 3-D thermal conduction capability. SOLID70 element has eight nodes with a single degree of freedom and temperature at each node. It is capable of good transient thermal analysis.

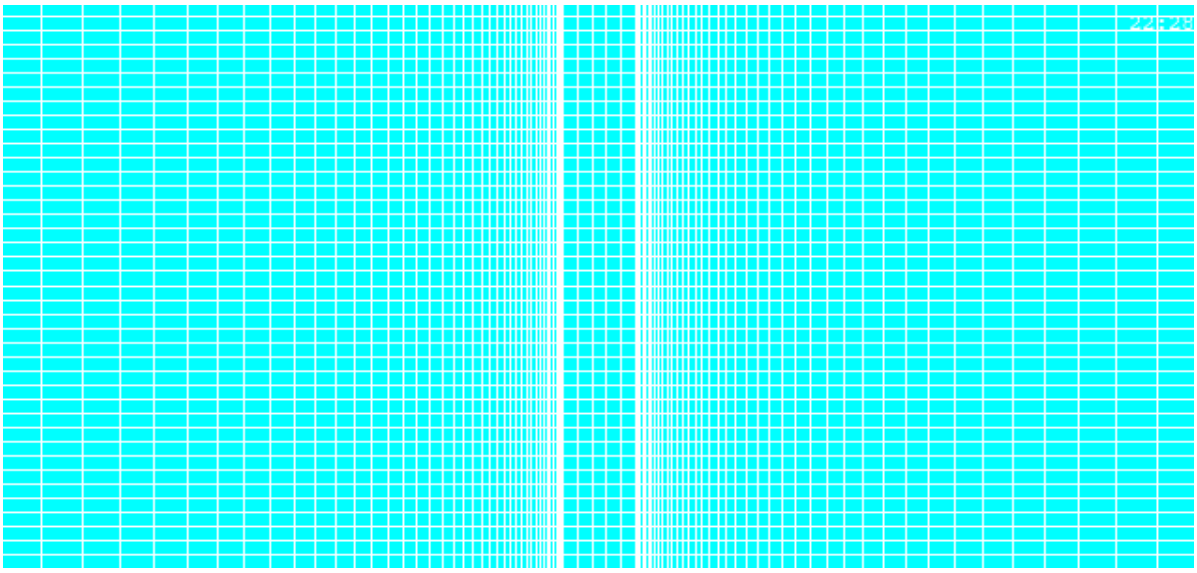

Fig. 2 Mesh Geometry of the Specimen

4.2.1 Mesh Model

The Fine meshing is used in the welding region to get the accurate temperature. In welding region the temperature is very high and change at very minimum distance means variation of temperature is more hence in the area of fusion zone and heat affected zone fine and uniform meshing is done. The variation of temperature is less in base metal hence course meshing is done at the base metal to reduce the computation time. The base metal has increasing mesh size (Fig.2) but in the fusion zone the size of element is fixed to 1.25 x 1.2 x 5 mm^3. Total number of nodes after meshing is 14104.

4.2.2 Heat Source Model

We all know the amount of total heat supplied is not fully absorbed by the material because the some of heat get loss to environment. The Heat generation per unit volume is calculated with the help of the equation given:

$$\boldsymbol{Q = \frac{\eta P}{v}} \tag{7}$$

η = absorption coefficient of the material, P = Power Supplied to the Weld
v = Volume of the element used in modeling. Q = Total heat generated per unit volume.

Absorption coefficient 5.32% was calculated by back substitution method in the heat source model in equation (7). [Ravisankaret et. al[30]].

Chapter-5

5. RESULTS AND DISCUSSION

The temperature distribution and the temperature distribution profile curve are numerically evaluated with the help of ANSYS APDL software using Finite Element Model (FEM). In this numerical method of evaluation the varying Power and Welding Speed are used for thermal analysis. The Power used in this analysis is 300 W, 400 W and 500 W and the varying welding speed are used as 60 mm/min, 120 mm/min and 180 mm/min. By using these parameter we find that the best combinations of parameter (500 W and 120 mm/min) which gives better weld penetration and good temperature distribution.

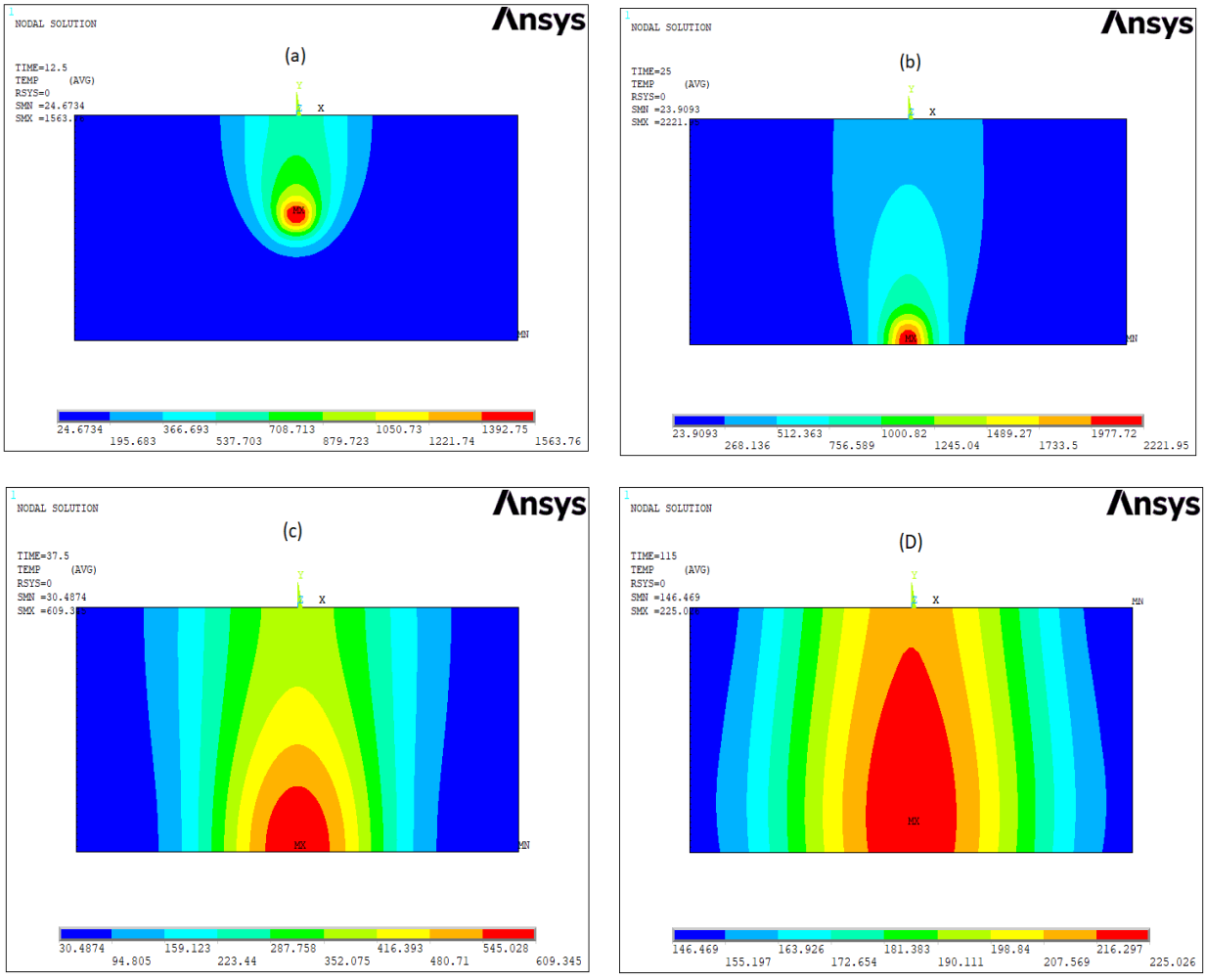

Fig.3 Temperature field distribution at (500 W and 120 mm/min) at different time

The temperature distribution is described in the above figure with respect to time for power 500 W and welding speed 120 mm/min. In this figure we can see that first temperature increases up to 25 sec (Fig. 3.b) and then decreases hence we can conclude that during welding process temperature increases with time and when welding completed then it decreases to ambient temperature.

In above Fig (3.a,b) shows temperature distribution during heating phase and Fig (3.c,d) shows the temperature distribution during cooling phase. One thing we also note from Fig(3.c,d) that during

cooling phase the temperature of base metal get increases because during cooling heat decreases at the weld line and these heat moves to base metal through conduction to increase the temperature of the base metal and some heat also dissipate through convection and radiation to the environment.

Temperature distribution and profile curve with the variation welding parameters are explained below:

5.1 Variation with Welding Power (P)

The welding power is very important parameters in welding process. This power decides that how much heat is generated during welding. The power we input is not completely generate heat at the weld some of heat gets absorbed by the material. This absorption is explained earlier in the heat source mode.

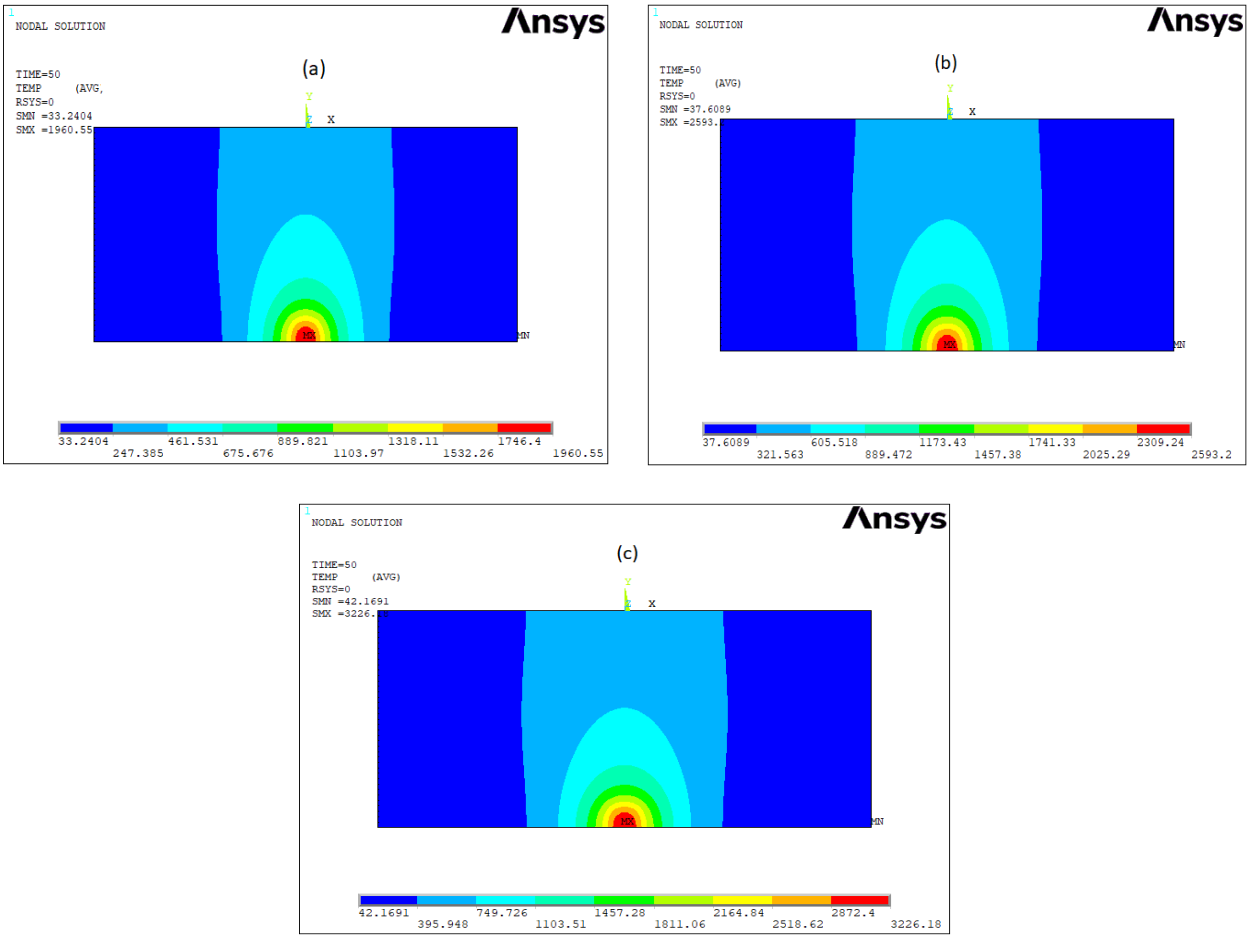

Fig.4 Temperature field distribution at 10th step at varying Welding Power

The temperature field distribution at various welding power(300-500W) and velocity of 60 mm/min at 10th step is shown in above figure. From there we can see clearly that the temperature is increases with increasing of wlding power. Fig(4a) shows the peak temperature of 1960.5 ^{o}C at 300 W, Fig(4b) shows the peak temperature of 2593.2 ^{o}C at 400W and Fig(4c) shows the peak temperature of 3226 ^{o}C at 500 W. Hence we conclude that temperature is increases when we increase the welding power.

The welding plate with size is shown below all the profile curve explained further according with this figure(5). The dimension in X-direction and Y-direction ,welding line and welding direction are clearly mentioned.

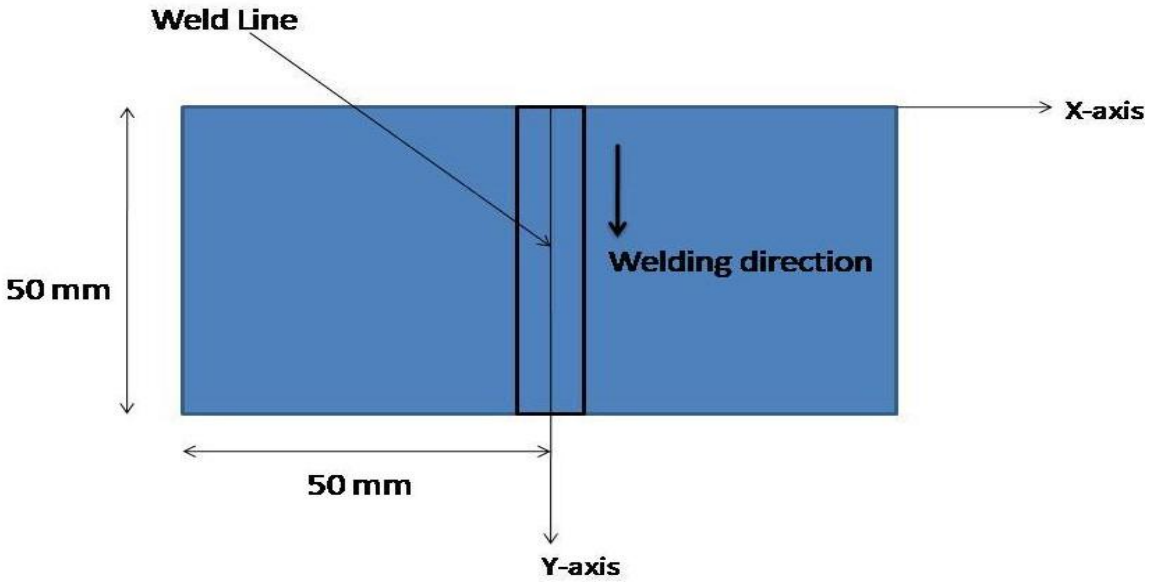

Fig.5 Welding plates of size 50mm x 50mm x 5 mm with butt joint

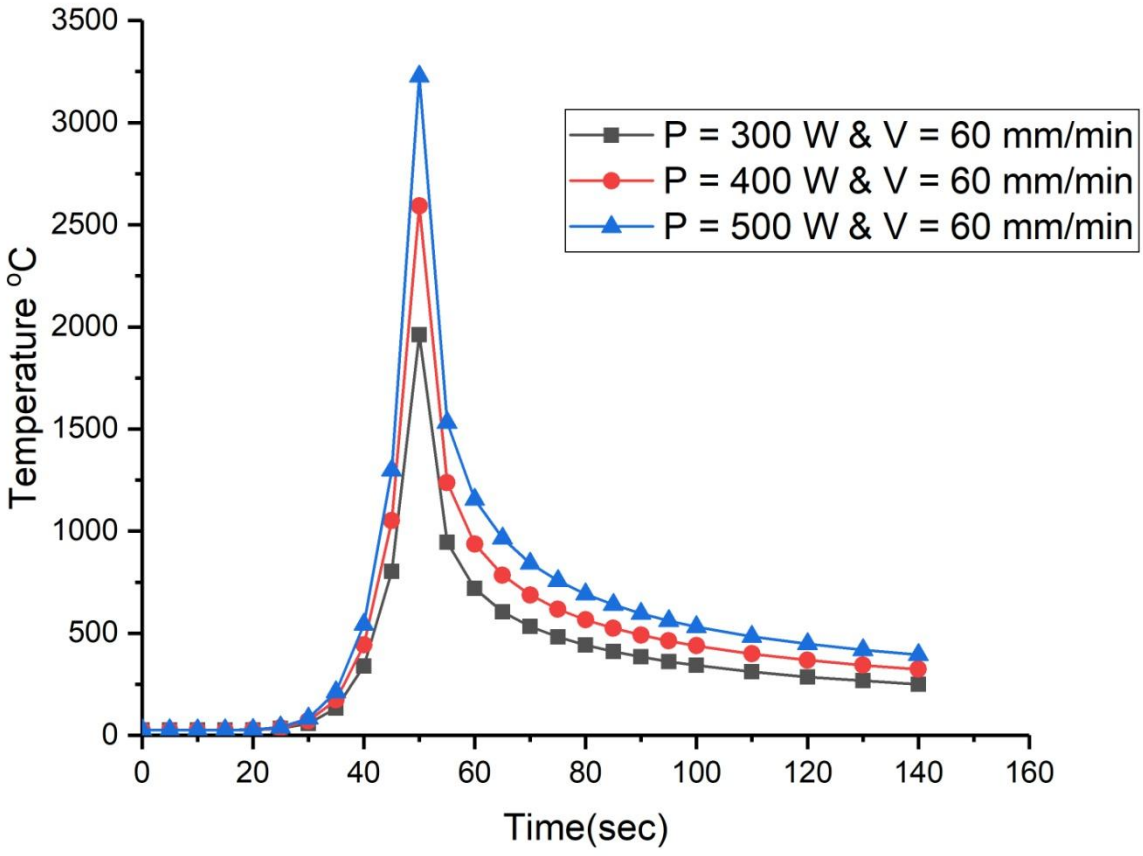

Fig.6 Temerature distribution profile curve with respect to time at node 87

The temperature distribution profile curve with time at various welding power(300-500W) and constant welding speed (60 mm/min) at node number 87 is shown in fig(6). From this curve we can observed that the peak temperature increases with increase in weling power and one thing we also note that the peak temperature at each power reases at the same time because of the welding speed, if the welding speed is constant the time taken to weld in each case is same.

When temperature reases at maximum point then it first decreases exponentially and after that it reaches the ambient temperature slowly. One thing we also note that during cooling phase the curve which has maximum welding power is above and the curve with lower welding power is at the lower side hence we can conclude from this is the weld with more welding power takes more time to reach to the room temperature because heat generated is more and welding with lower welding power takes less time to reach to the room temperature because less heat generation.

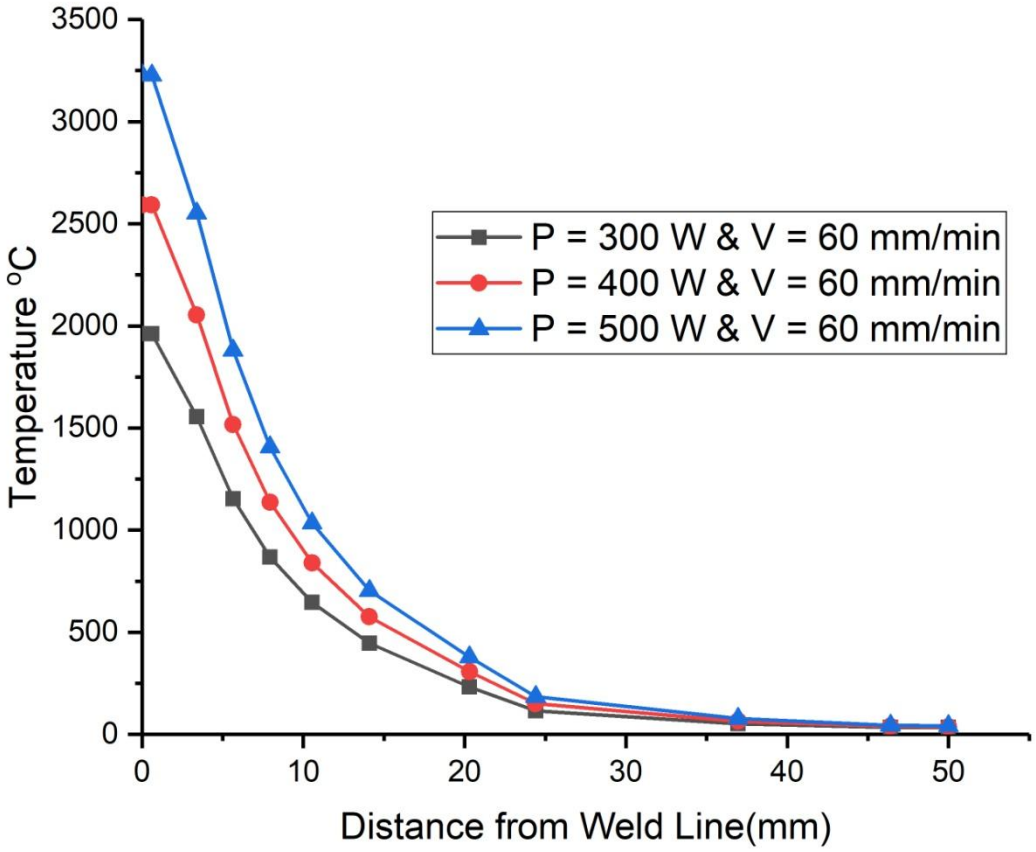

Fig.7 Temperature profile curve with respect to distance from weld line at time 50 sec

The temperature profile at step 10^{th} and time 50 sec with distance from weld line (X) at Y 50 mm (see fig.5) at different welding power and constant welding speed are shown in the above figure. In this curve we see that the temperature decreases with increase in distance from the weld line and almost constant after some distance. The temperature at the weld line is greater for larger power taken for welding. The variation of temerature with distance from weld line is more it means that

small change in distance gives large change in temperature upto approx 25 mm and after that the variation of temperature is low and then after, it seems almost constant.

5.2 Variation with welding speed (V)

Welding speed is another important parameters in the welding process. Weld speed helps to decide how faster we achieve the weld. The thermal analysis (the distribution of the temperature and also temperature profile curve) with respect to the welding speed(60-180 mm/min) and constant power of 500 W is explained here.

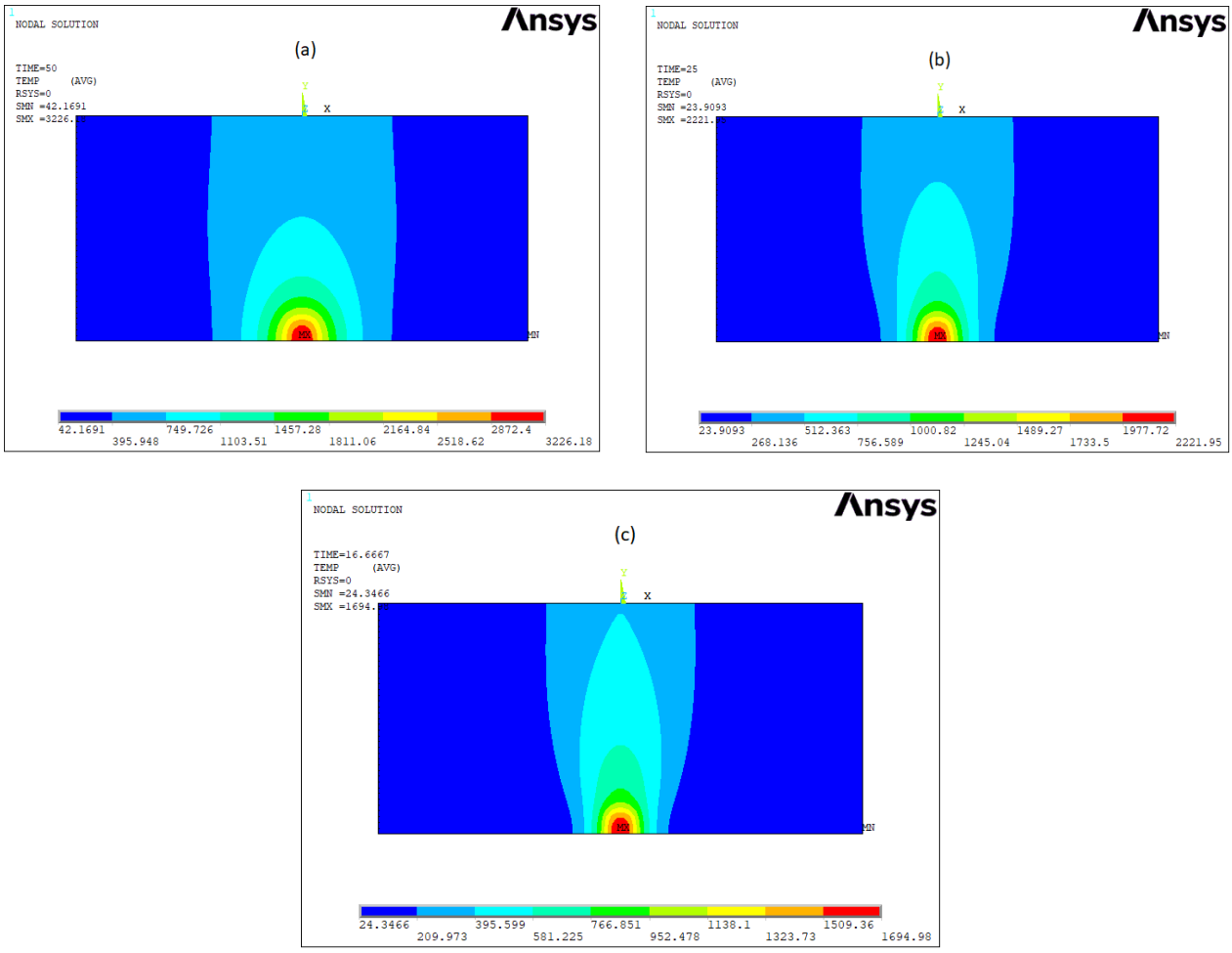

Fig.8 Temperature field distribution at 10th step at varying Welding Speed

The Temperature field distribution at 10th step with varying welding speed (60,120,180 mm/min) and constant power of 500 W is shown above. Fig(8.a) has welding speed of 60 mm/min, it shows the peak temperature of 3226 ^{o}C, fig(8.b) has welding speed of 120 mm/min, it shows the peak temperature of 2221.95 ^{o}C and fig(8.c) has welding speed of 180 mm/min and it shows the peak temperature of 1694.98 ^{o}C. It clearly seems that the temperature is increases with decrease in welding speed. Hence we can conclude from above statment that the temperature is inversely

proportional to the welding speed, if we increase the welding speed leaving all parameters of the weld constant temperature of the weld decreases.

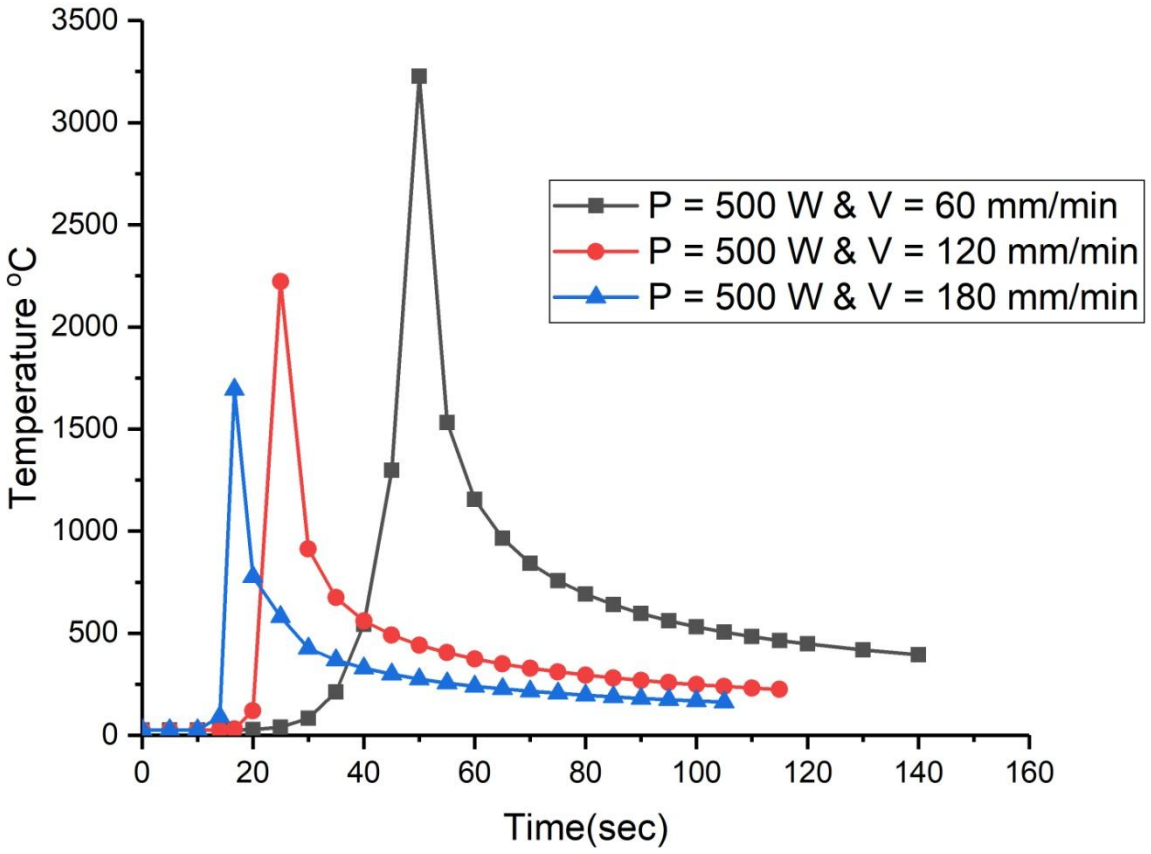

Fig.9 Temperature distribution curve with time at node 87

In the above temperature distribution curve at node 87 of different welding speed(60-180 mm/min) and constant power of 500 W, we see that peak temperature decreases with increase in welding speed. The temperature reaches its maximum value at different time because of the different welding speed. Welding with speed 60 mm/min reaches its maximum temerature value at the time of 50 sec, welding with speed 120 mm/min takes 25 sec to reach its maximum temperature and welding with speed 180 mm/min takes only 16.67 sec to reach its maximum temperature value. Hence the maximum welding speed leads to gain highest temperature at minimum time but heat generated with maximum welding speed is minimum because we see that minimum peak temperature is for the maximum welding speed.

We see that the curve first moves at constant temperature then rapidely increases at a certain time because when the heat is away from the node 87 then the temperature is constant then increases rapidely when the heat source come to it. The heat source reaches to this node at different time

because the welding speed is different. When the curve reases its maximum value and after that during cooling phase it decrease rapidely up to a certain period of time and the after slowly decreases We can see that welding with the speed of 180 mm/min curve are at the lower from the rest all during cooling phase hence we can say that the maximum welding speed parameters weld takes less time to reach at room temperature because of less heat generated.

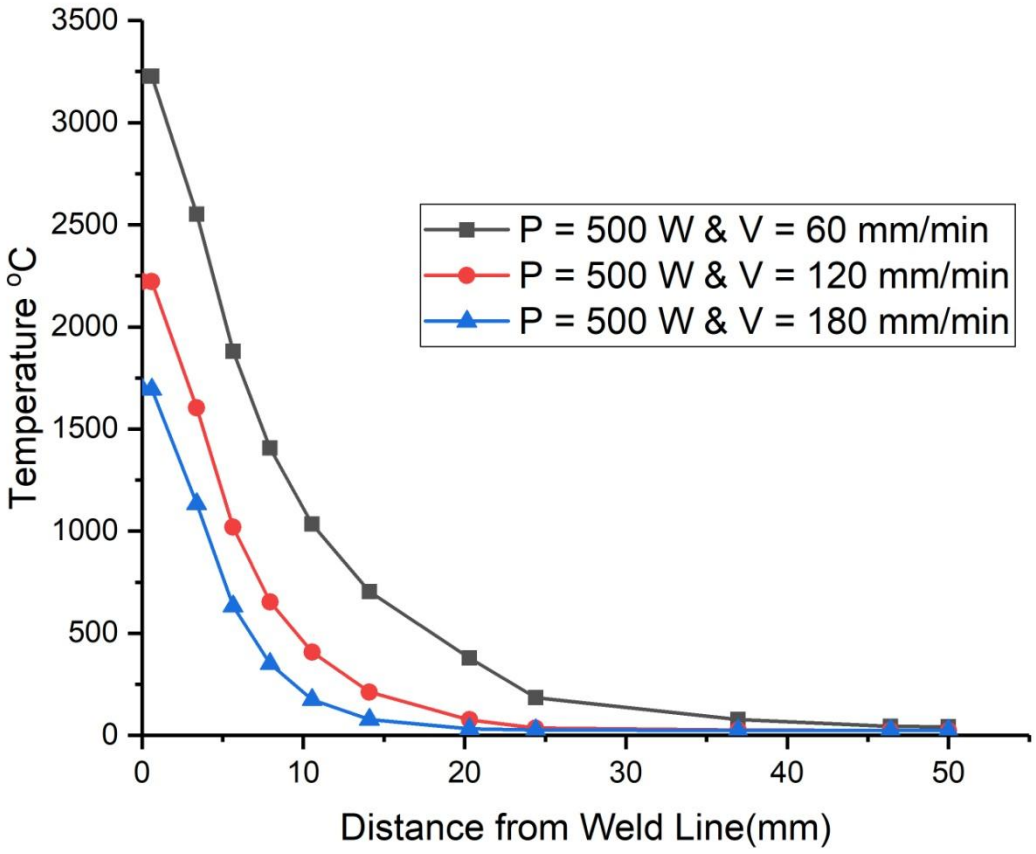

Fig.10 Temperature profile curve with respect to distance from weld line

The temperature curve with different welding speed and and fixed welding power at step 10th with varying distance in X that is from the weld line at Y 50 mm (see Fig.5) are shown above. In this curve temperature is decreases with increase in distance from the weld line. Weld with lower welding speed that is 60 mm/min has more temperature at welding line and welding with the higher speed that is 180 mm/min has less temperature at the weld line and all curves are decreases with increase in distance.

5.3 Analysis of Fusion zone and Heat affected zone

Generally the weld joint are divided into two main zone the first one is Fusion Zone (FZ) and the second one is the Heat affected Zone (HAZ). The fusion zone and heat affected zone plays a important role to determine the mechanical properties of weld specimen. The weld zone where the material is melted to join two different or same type of material is the fusion zone and out side it

there is a haet affected zone and out side HAZ there is base metal. The HAZ is considered as transition zone because of its microstructure, it composed with the microstructure of both(base metal and fusion zone). The most critical section is the heat affected zone because chance of failure is more when applied a larger tensile load. Heat affected zone is also further divided into different zone accordance with the size of grins formed.

HAZ (heat affected zone) exhibited larger grains and the FZ (Fusion Zone) presented more refined grains as compared to base metal **(**Bo QIN et. al [11]). Hence the heat affected zone is the most weaker zone. In this thesis we study the size of fusion and heat affected zone with variation of welding power and the welding speed.

In AISI 304 phase transformation would occur at temperature ranges between 950 to 1440 ^{o}C under equilibrium condition. Hence the study of size of weld between these temperature range with different welding power and welding speed are performed.

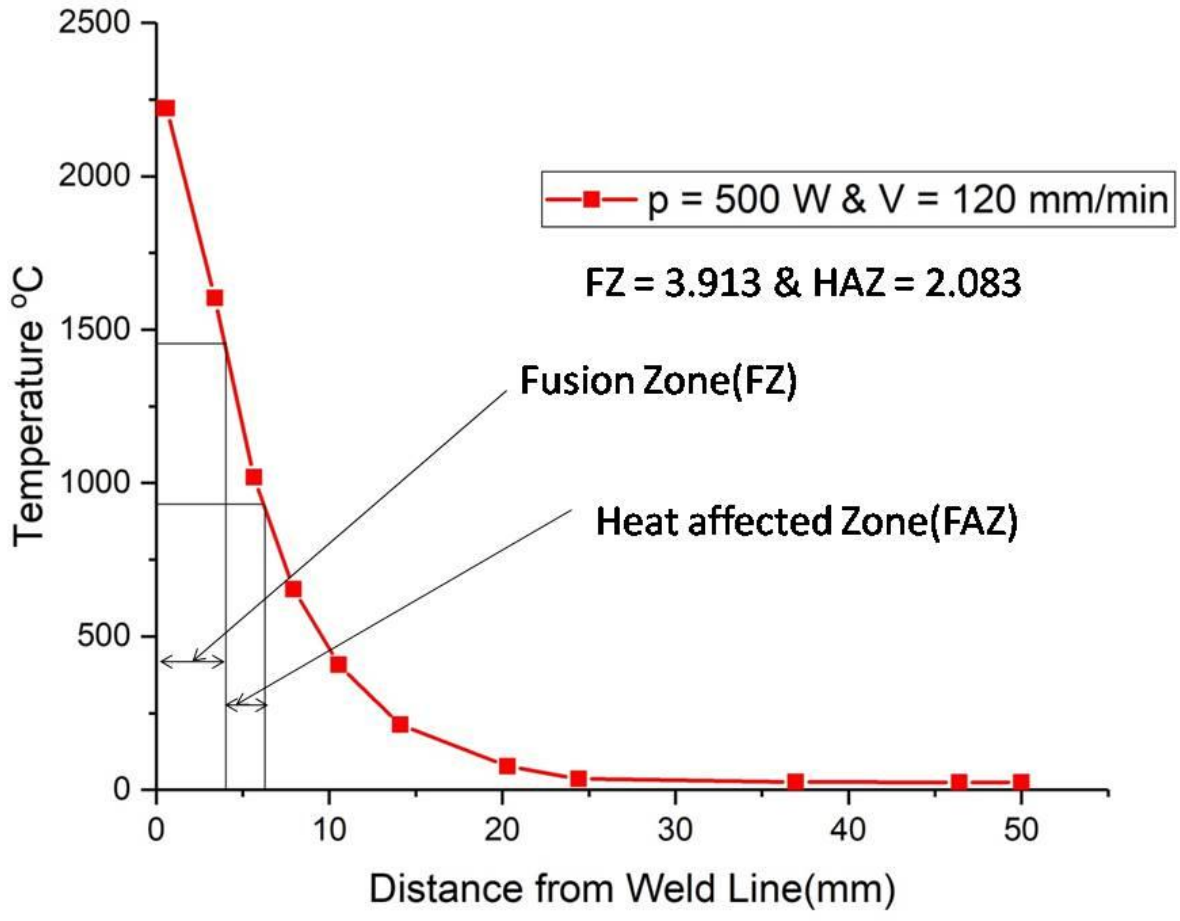

Fig.11 Size of FZ and HAZ in butt weld at Power 500 W and welding speed 120 mm/min

First the temperature vs distance from weld line curve are plotted, in this curve the peak temperature is 2221.95 ^{o}C. Locate a point 1440 ^{o}C in the graph the distance correspond to this point is 3.913 mm, this distance is the size of fusion zone.

We locate a another point of 950 ^{o}C in the above graph the distance correspond to it is 5.996 mm, this is the distance from weld line, substract the size of fusion zone from it then we get the value of 2.083 mm, this is the size of heat affected zone.

In this way we calculate different size of fusion and heat affected zone with varying welding power and welding speed and the graph are plotted to study the size of it with respect of these parameters.

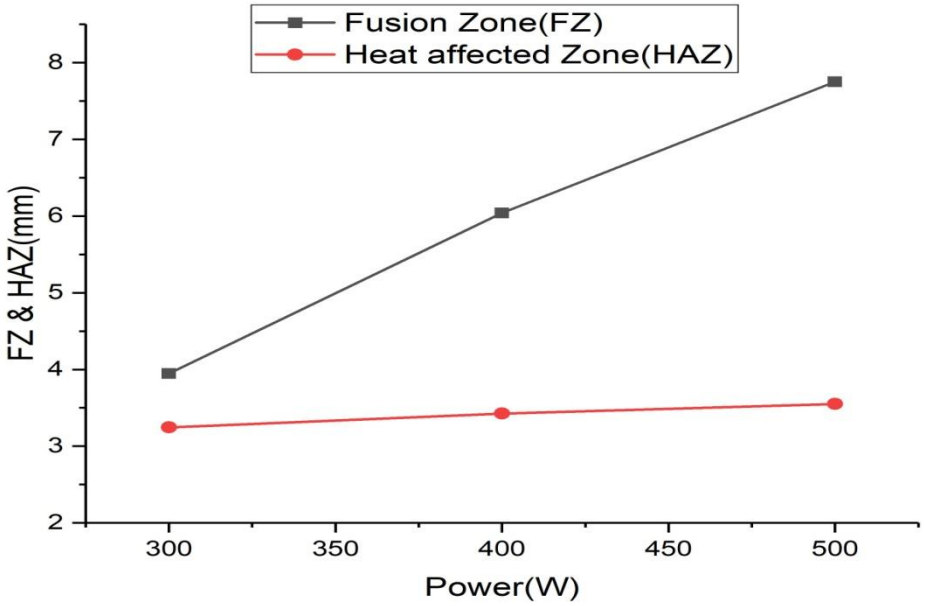

Fig.12 Size of FZ and HAZ with Welding Power

The size fusion zone and heat affected zone with varying welding power are plote in the above curve. From there we see the size of both fusion and heat affected zone are increased with increasing in the welding power because when welding power is increased then the heat generated is also increased. Hence the increased heat increase the size of fusion zone and heat affected zone. One thing we also note from the above graph that the size of fusion zone increase with greater rate as compared to heat affected zone.

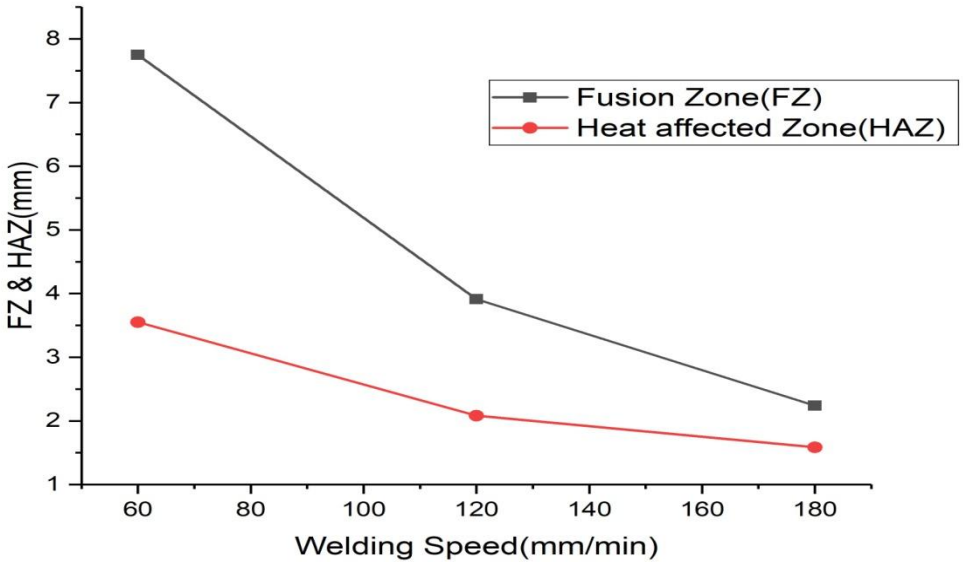

Fig.13 Size of FZ and HAZ with welding speed

The size of fusion and heat affected zone are ploted in the fig.13 with varying welding speed and pattern are studied. From this curve we found that the size of both fusion and heat affected zone decreases with increase in welding speed because when the welding speed is increases then the heat generation is less hence less heat decrease the size of fusion and heat affected zone.

5.4 Variation of Temperature at various point

(a) Away from welding line

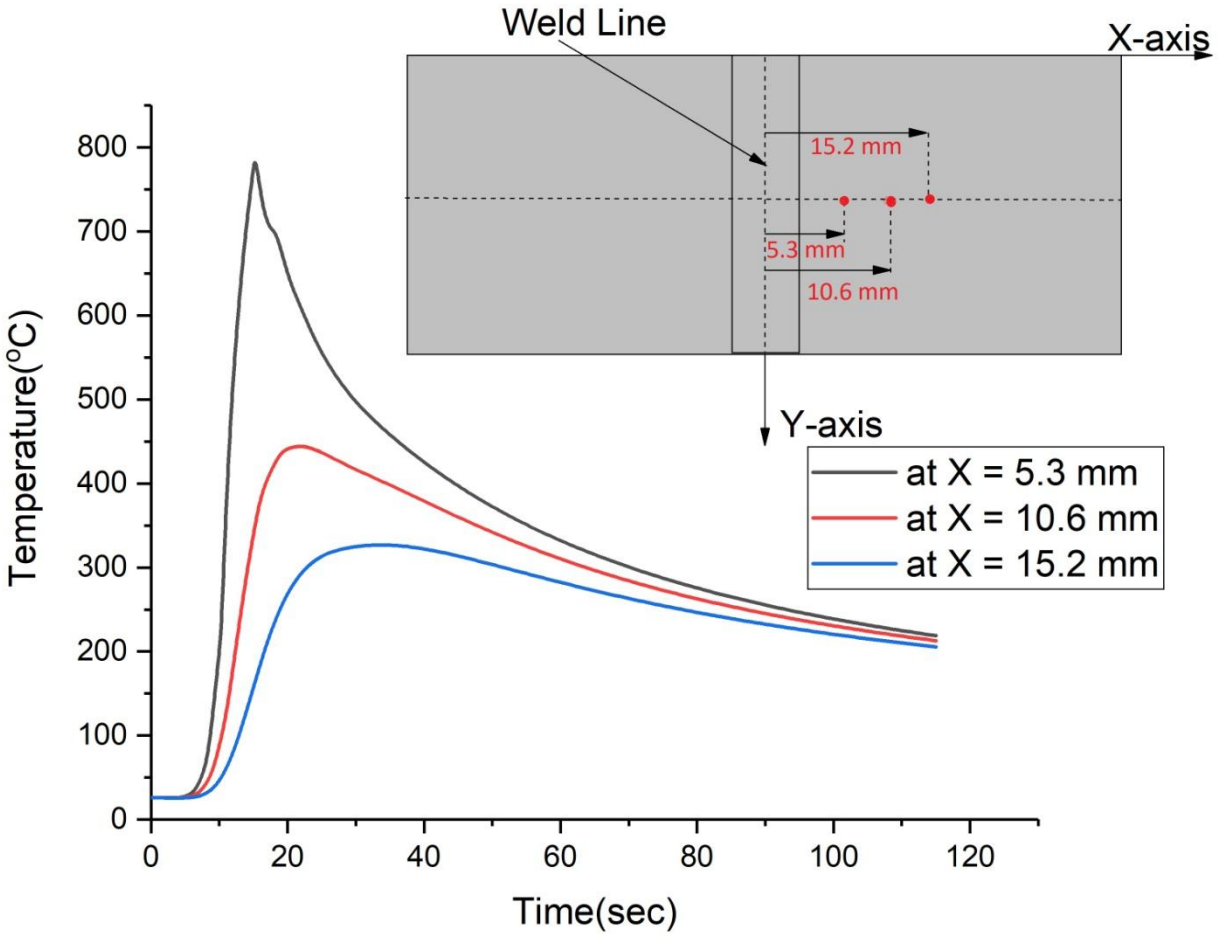

Fig.14 Temperature profile curve at different point from central line away from welding line at P (500W) and V(120 mm/min)

The above temperature curve with respect to time are ploted at various point at node 4514, 4124 and 392 from central line(Y=25 mm) away from weld line at welding power 500W and and welding speed 120 mm/min and nature of curve are studied. The peak temperature at X=5.3 mm, 10.6 mm and 15.2 mm at time 15.2 sec, 21.9 sec and 34 sec are 781.874, 444.155 and 326.889 ^{o}C respctively. We see that as the distance increased from from the welding line the peak temperature are decreased. From above curve we can also say that heat flows away from the weld line because as the time passes the point away from the weld line gets heat and temperature rises up but gets less heat as compared to initial point.

b) Along the weld line

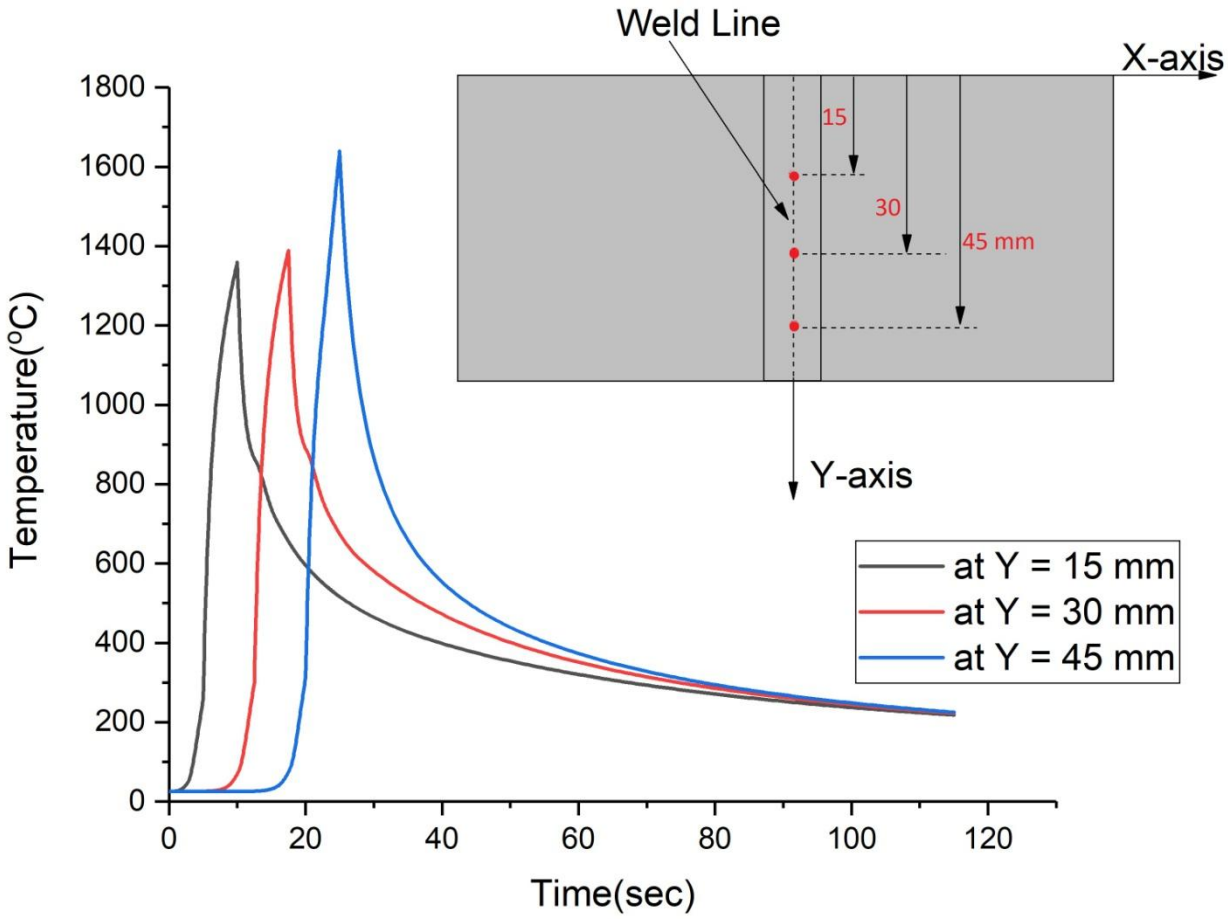

Fig.15 Temperature curve at different point along the central line at P(500W) and V(120 mm/min)

In this figure(15) a temperature profile curve with respect to time is ploted at welding power 500W and welding speed 120 mm/min at different node like 3225, 3297 and 96 along the weld line. The peak temperature at Y=15 mm, 30 mm and 45 mm at time 10 sec, 17.5 sec and 25 sec are 1359.1, 1388.98 and 1639.53 ^{o}C respectively. Hence we can say that as distance increases along the weld line the peak temperature also increases. We can also found that as the distance increases along weld line then the time taken to node to achieve the peak temperature is also increases because as the distance increases along the weld line the heat sources takes more time to reach that point to increase that temperature.

5.5 Experimental validation

The result obtained from numerical simulation is validated with experimental result performed by Ravisankar et. al [30]. They used the k- type thermocouple at various locations with welding speed of 60 mm/min and 300 W Power. The maximum temperature found at various locations by numerical simulation and maximum temperature obtained experimentally is shown in graph below:

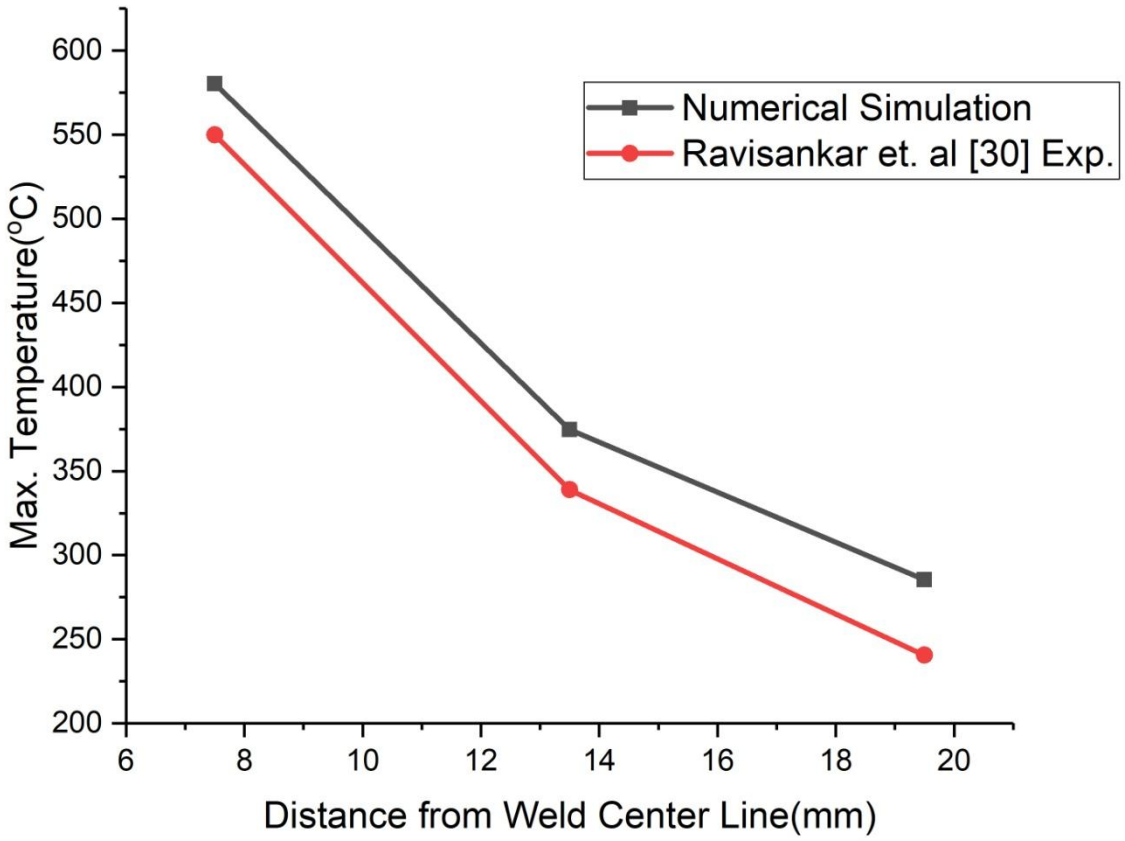

Fig.16 Validation of Peak temperature distribution obtained numerically with experimental result at various locations from weld center line.

The curve are plotted taking maximum peak temperature from numerical and experimental at points 7.5 mm, 13.5 mm and 19.5 mm away from weld center line. It is observed from above graph that the result obtained from numerical simulation and experimental match well and the minimum error of 5.17% at the location 7.5 mm and maximum at the location 19.5 mm away from weld center line are achieved.

Chapter-6

6. CONCLUSION

The current study investigates the TIG Welding process parameters like welding speed and power and their effect on temperature distribution and temperature profile curves of the butt joint of AISI 304 material. The result obtained from numerical simulation is validated with the experimental result in fig.16 which gives good agreement between them. From the above investigation the following conclusions can be drawn:

- It has been found that the increase in welding power increase the peak temperature of the weld and increase in the welding speed decrease the heat and also decrease the peak temperature.
- The maximum peak temperature is obtained at the welding of 500 W and 60 mm/min is 3226^{o}C and minimum peak temperature obtained at 500 W and 180 mm/min is 1694.98^{o}C.
- The minimum fusion zone and heat affected zone of 2.24 mm and 1.586 mm respectively are found at 500 W and 180 mm/min.
- The best combinations of parameter (500 W and 120 mm/min) which gives better weld penetration and good temperature distribution.
- The peak temperature decreases in increases distance from the weld line in each case.
- The validation of result obtained from numerical simulation and with experimental result at various locations away from the weld center line gives good agreement between them and the minimum error of 5.17% are found at the point 7.5 mm away from weld center line.

Future scope of work

In the present study thermal analysis is done, there is a scope of structural analysis for the study of residual stress and residual deformation. In this thesis the variation of welding power and welding speed was studied but we can also vary the current and welding speed and accordance with it a 3-D model will be created for the study of thermo-mechanical analysis.

REFRENCES

[1] Pydi, H.P., Pasupulla, A.P., Vijayakumar, S. and Agisho, H.A., 2022. Study on microstructure, behavior and Al_2O3 content flux A-TIG weldment of SS-316L steel. *Materials Today: Proceedings*, *51*, pp.728-734.

[2] Zala, A.B., Jamnapara, N.I., Sasmal, C.S., Sam, S. and Ranjan, M., 2022. Study of microstructure & mechanical properties of TIG welded aluminized 9Cr-1Mo steel. *Fusion Engineering and Design*, *176*, p.113038.

[3] Panda, S.S., 2021. Characterisation of Cu–Al alloy lap joint using TIG Welding. *CIRP Journal of Manufacturing Science and Technology*, *35*, pp.454-459.

[4] Pandya, D., Badgujar, A. and Ghetiya, N., 2021. Effect of hydrogen additions to shielding gas on activated TIG austenitic stainless steel weld. *Materials Today: Proceedings*, *47*, pp.1025-1029.

[5] Kavitha, K.R., Kumar, G., Srinivas, G.L., Mercy, J.L., Sivashankari, P. and Joy, N., 2021. Evaluation study of mechanical properties of dissimilar materials through TIG welding process. *Materials Today: Proceedings*, *44*, pp.3894-3897.

[6] Nehar Ansari, Dr.Lokesh Singh., 2019. Review paper on TIG (tungsten inert gas welding) or GTAW(gas tungsten arc welding*). International Journal of Innovations in Engineering and Science, Vol 4, No.12, 2019*

[7] Satputaley, S.S., Waware, Y., Ksheersagar, K., Jichkar, Y. and Khonde, K., 2021. Experimental investigation on effect of TIG welding process on chromoly 4130 and aluminum 7075-T6. *Materials Today: Proceedings*, *41*, pp.991-994.

[8] Bansal, A., Kumar, M.S., Shekhar, I., Chauhan, S. and Bhardwaj, S., 2021. Effect of welding parameter on mechanical properties of TIG welded AA6061. *Materials Today: Proceedings*, *37*, pp.2126-2131.

[9] Omoniyi, P., Mahamood, M., Jen, T.C. and Akinlabi, E., 2021. TIG welding of Ti6Al4V alloy: Microstructure, fractography, tensile and microhardness data. *Data in Brief*, *38*, p.107274.

[10] Ramakrishnan, A., Rameshkumar, T., Rajamurugan, G., Sundarraju, G. and Selvamuthukumaran, D., 2021. Experimental investigation on mechanical properties of TIG welded dissimilar AISI 304 and AISI 316 stainless steel using 308 filler rod. *Materials Today: Proceedings*, *45*, pp.8207-8211.

[11] Bo, Q.I.N., Yin, F.C., Zeng, C.Z., Xie, J.C. and Jun, S.H.E.N., 2019. Microstructure and mechanical properties of TIG/A-TIG welded AZ61/ZK60 magnesium alloy joints. *Transactions of Nonferrous Metals Society of China*, *29*(9), pp.1864-1872.

[12] Baghel, A., Sharma, C., Rathee, S. and Srivastava, M., 2021. Activated flux TIG welding of dissimilar SS202 and SS304 alloys: Effect of oxide and chloride fluxes on microstructure and mechanical properties of joints. *Materials Today: Proceedings*, *47*, pp.7189-7195.

[13] Kulkarni, A., Dwivedi, D.K. and Vasudevan, M., 2020. Microstructure and mechanical properties of A-TIG welded AISI 316L SS-Alloy 800 dissimilar metal joint. *Materials Science and Engineering: A*, *790*, p.139685.

[14] Qin, Q., Zhao, H., Li, J., Zhang, Y., Zhang, B. and Su, X., 2020. Microstructures and mechanical properties of TIG welded Al-Mg2Si alloy joints. *Journal of Manufacturing Processes*, *56*, pp.941-949.

[15] Kumar, K., Deheri, S.C. and Masanta, M., 2019. Effect of activated flux on TIG welding of 304 austenitic stainless steel. *Materials Today: Proceedings*, *18*, pp.4792-4798.

[16] Hazari, H.R., Balubai, M., Kumar, D.S. and Haq, A.U., 2019. Experimental investigation of TIG welding on AA 6082 and AA 8011. *Materials Today: Proceedings*, *19*, pp.818-822.

[17] Shi, J., Song, G. and Chi, J., 2018. Effect of active gas on weld appearance and performance in laser-TIG hybrid welded titanium alloy. *International Journal of Lightweight Materials and Manufacture*, *1*(1), pp.47-53.

[18] Junaid, M., Baig, M.N., Shamir, M., Khan, F.N., Rehman, K. and Haider, J., 2017. A comparative study of pulsed laser and pulsed TIG welding of Ti-5Al-2.5 Sn titanium alloy sheet. *Journal of Materials Processing Technology*, *242*, pp.24-38.

[19] Samiuddin, M., Li, J.L., Taimoor, M., Siddiqui, M.N., Siddiqui, S.U. and Xiong, J.T., 2021. Investigation on the process parameters of TIG-welded aluminum alloy through mechanical and microstructural characterization. *Defence Technology*, *17*(4), pp.1234-1248.

[20] Vidyarthy, R.S. and Dwivedi, D.K., 2019. Weldability evaluation of 409 FSS with A-TIG welding process. *Materials Today: Proceedings*, *18*, pp.3052-3060.

[21] Chen, C., Fan, C., Cai, X., Lin, S., Liu, Z., Fan, Q. and Yang, C., 2019. Investigation of formation and microstructure of Ti-6Al-4V weld bead during pulse ultrasound assisted TIG welding. *Journal of Manufacturing Processes*, *46*, pp.241-247.

[22] Jun, S.H.E.N., Zhai, D.J., Kai, L.I.U. and Cao, Z.M., 2014. Effects of welding current on properties of A-TIG welded AZ31 magnesium alloy joints with TiO2 coating. *Transactions of Nonferrous Metals Society of China*, *24*(8), pp.2507-2515.

[23] Lu, S.P., Qin, M.P. and Dong, W.C., 2013. Highly efficient TIG welding of Cr13Ni5Mo martensitic stainless steel. *Journal of Materials Processing Technology*, *213*(2), pp.229-237.

[24] Song, J.L., Lin, S.B., Yang, C.L. and Fan, C.L., 2009. Effects of Si additions on intermetallic compound layer of aluminum–steel TIG welding–brazing joint. *Journal of Alloys and Compounds*, *488*(1), pp.217-222.

[25] Singh, S.R. and Khanna, P., 2021. A-TIG (activated flux tungsten inert gas) welding:–A review. *Materials Today: Proceedings*, *44*, pp.808-820.

[26] Singh, N.K., 2017. Performance of activated TIG welding in 304 austenitic stainless steel welds. *Materials Today: Proceedings*, *4*(9), pp.9914-9918.

[27] Sharma, P. and Dwivedi, D.K., 2019. A-TIG welding of dissimilar P92 steel and 304H austenitic stainless steel: mechanisms, microstructure and mechanical properties. *Journal of Manufacturing Processes*, *44*, pp.166-178.

[28] Bhadra, R., Pankaj, P., Biswas, P. and Dixit, U.S., 2019. Thermo-mechanical analysis of CO2 laser butt welding on AISI 304 steel thin plates. *International Journal of Steel Structures*, *19*(1), pp.14-27.

[29] Kumar, P., Kumar, R., Arif, A. and Veerababu, M., 2020. Investigation of numerical modelling of TIG welding of austenitic stainless steel (304L). *Materials Today: Proceedings*, *27*, pp.1636-1640.

[30] Ravisankar, A., Velaga, S.K., Rajput, G. and Venugopal, S., 2014. Influence of welding speed and power on residual stress during gas tungsten arc welding (GTAW) of thin sections with constant heat input: A study using numerical simulation and experimental validation. *Journal of Manufacturing Processes*, *16*(2), pp.200-211.

[31] Zeng, Z., Li, X., Miao, Y., Wu, G. and Zhao, Z., 2011. Numerical and experiment analysis of residual stress on magnesium alloy and steel butt joint by hybrid laser-TIG welding. *Computational Materials Science*, *50*(5), pp.1763-1769.

[32] Vakili-Tahami, F., Majnoun, P. and Akhlaghifar, N., 2017. Numerical Simulation of the T-shape fillet welds of 304 and 1020 Steel plates. *UPB Sci. Bull*, *79*, pp.103-118.